REPORT DOCUMENTATION PAGE

Form Approved OMB NO. 0704-0188

1. REPORT DATE (DD-MM-YYYY)	2. REPORT TYPE	3. DATES COVERED (From - To)
18-11-2019	Final Report	21-Aug-2015 - 20-Aug-2019

4. TITLE AND SUBTITLE
Final Report: Research and Education on Lightweight and Flexible Photo-/Thermo-Electric Multi-Functional Materials

5a. CONTRACT NUMBER
W911NF-15-1-0422

5b. GRANT NUMBER

5c. PROGRAM ELEMENT NUMBER
106012

6. AUTHORS

5d. PROJECT NUMBER

5e. TASK NUMBER

5f. WORK UNIT NUMBER

7. PERFORMING ORGANIZATION NAMES AND ADDRESSES
Norfolk State University
700 Park Avenue
McDemmond Center for Applied Research, Suite 601
Norfolk, VA 23504 -8060

8. PERFORMING ORGANIZATION REPORT NUMBER

9. SPONSORING/MONITORING AGENCY NAME(S) AND ADDRESS (ES)
U.S. Army Research Office
P.O. Box 12211
Research Triangle Park, NC 27709-2211

10. SPONSOR/MONITOR'S ACRONYM(S)
ARO

11. SPONSOR/MONITOR'S REPORT NUMBER(S)
67279-CH-REP.27

12. DISTRIBUTION AVAILIBILITY STATEMENT
Approved for public release; distribution is unlimited.

13. SUPPLEMENTARY NOTES
The views, opinions and/or findings contained in this report are those of the author(s) and should not contrued as an official Department of the Army position, policy or decision, unless so designated by other documentation.

14. ABSTRACT

15. SUBJECT TERMS

16. SECURITY CLASSIFICATION OF:			17. LIMITATION OF ABSTRACT	15. NUMBER OF PAGES	19a. NAME OF RESPONSIBLE PERSON
a. REPORT	b. ABSTRACT	c. THIS PAGE			Sam-Shajing Sun
UU	UU	UU	UU		19b. TELEPHONE NUMBER 757-823-2993

RPPR Final Report
as of 13-Jan-2020

Agency Code:

Proposal Number: 67279CHREP **Agreement Number: W911NF-15-1-0422**
INVESTIGATOR(S):

Name: Sam-Shajing Sun
Email: ssun@nsu.edu
Phone Number: 7578232993
Principal: Y

Organization: **Norfolk State University**
Address: 700 Park Avenue, Norfolk, VA 235048060
Country: USA

DUNS Number: 074754805 EIN: 546002808
Report Date: 20-Nov-2019 Date Received: 18-Nov-2019
Final Report for Period Beginning 21-Aug-2015 and Ending 20-Aug-2019
Title: Research and Education on Lightweight and Flexible Photo-/Thermo-Electric Multi-Functional Materials
Begin Performance Period: 21-Aug-2015 **End Performance Period:** 20-Aug-2019
Report Term: 0-Other

Submitted By: Sam-Shajing Sun Email: ssun@nsu.edu
Phone: (757) 823-2993

Distribution Statement: 1-Approved for public release; distribution is unlimited.

STEM Degrees: 20 **STEM Participants:** 25

Major Goals: The short term objectives of this proposed project is to investigate and develop certain molecular or organic/polymeric hybrid composite systems (via molecular structure and frontier orbital systematic optimization approaches) for high efficiency photoelectric, thermoelectric, or photo-/thermo-electric multi-functional conversion systems. The long-term objectives of the project include investigation and elucidation of the fundamental mechanisms of photo- and thermo- induced electron transfer processes in molecular or organic/polymeric hybrid materials systems, for instance, the correlations between the molecular frontier orbitals, molecular structures, solid state morphologies, to electron transfers and materials bulk photo- and thermo- electric conversions. Another key long term objective of the project is the education and training of future generation scientists or technical work force on the subject matter.

Accomplishments: 1) Progresses on Investigations of Thermoelectric(TE)/Photoelectric(PE) and Thermoelectric (TE)/Electroelectric(EE) Multi-Functional Materials

The PE/TE and TE/EE dual conversion and dual modulation materials and devices have been preliminary and successfully demonstrated. For example, in one PE/TE dual conversion polymer thin film sample, temperature can effectively modulate the photo detector while simultaneously light can effectively modulate the thermoelectric Seebeck coefficients of the same sample. The correlations of the frontier orbital levels and offsets versus electrical and thermoelectric properties of a series of PCBM:P3HT:dopant ternary composites were also evaluated. It was observed that strong electron accepting strength of the dopant can result in P3HT main chain aggregations even in solution. In the solid-state thin films, it was found that the presence of acceptors increases surface roughness and disrupt the crystallinity of P3HT or P3HT:PCBM thin films. As the orbital offsets (or energy barriers) between HOMO of P3HT and LUMO of dopants increases from F4-TCNQ to iodine to DDQ and finally to TCNQ, the electrical conductivity decreases (possibly due to energy barrier increases), the Seebeck coefficients increases (due to charge carrier density decreases), while the thermoelectric power factor and the thermoelectric figure of merit ZT initially decreases from F4-TCNQ to DDQ (possibly due to dominant electrical conductivity contribution decrease) and then increases slightly to TCNQ (possibly due to dominant Seebeck contribution increase). This work could be helpful to understand the mechanisms of chemical doping of conjugated polymers at the molecular level and their correlations to bulk thermoelectric properties for a variety potential applications.

2) Progresses on Development of a Novel DB-ffA Block Copolymer and Structure/Morphology/Property Correlation Studies of the DBfA Type Block Copolymers

A new benzene disulfide and di-fluorinated monomer 7b and new disulfide and di-fluorinated functionalized

conjugated polymer block ffA-b were successfully synthesized and characterized, but once the sulfides were oxidized into the desired sulfone acceptor form, the ffA-b become insoluble. Soluble analogues may be developed but that would involve synthetic adjustments from first synthetic step. The correlation studies between chemical structures, morphology, and electronic/optoelectronic properties of the DBfA systems that were developed earlier is being evaluated systematically. Important observations/conclusions include that 1) that DB1fA block copolymer containing one methylene unit exhibited the strongest PL quenching and the best optoelectronic property (The PL quenching of no-bridge DfA or DB2fA were much less); and 2) an intermediate thin film gran size or roughness appear to exhibit best optoelectronic performance in a DB1fA block copolymer.

3) Progresses on Investigations of a Series New Octabutoxy-Metal-Pthalocyannine Complexes (OB-MPc) for Optoelectronics

A series of soluble OB-MPc molecular dyes containing different metals have been successfully synthesized and characterized (via NMR, MALDI, electrochemistry, optical absorption and emission spectroscopies, etc). These OB-MPc molecular dyes have identical or similar chemical structures but different frontier orbital levels due to different metals present in the center of the molecule, i.e., they are ideal candidates for electron transfer studies as the reorganization energies can be assumed to be same or similar, but the electron transfer driving force would be different. Photoluminescence Stern-Volmer studies of these dyes paired with P3HT were carried out to evaluate photo induced charge separations between the dyes and P3HT. Preliminary results confirmed some key features of Marcus electron transfer curve, i.e., an inverted region was indeed observed.

Training Opportunities: Though only two graduate and two undergraduate student supports were originally budgeted and allocated in the project, during the entire project period, at least four PhD students, one master student, and over twenty (20) undergraduate students participated and were educated/trained in the awarded project. All participating students are majored in key STEM areas including materials science, chemistry, engineering, etc. One PhD degree dissertation (on research thrust 1) and one Master degree thesis (on research thrust 3) have already been completed/defended during the project period. Another PhD dissertation (on research thrust 2) is currently in final stage, and two additional PhD dissertations (on research thrust 1 related subjects) are on the pipeline. Most of the over twenty undergraduate student participants have already graduated with BS degrees in key STEM areas. Majority of the participating students are under-represented minority and/or female students. The first supported PhD graduate student who defended his PhD dissertation in summer 2018 was voted as our materials science PhD program's outstanding PhD student awardee. This PhD graduate has been offered several job offers from major high tech corporations/national labs since his graduation, and most importantly he also successfully won a prestigious NSF postdoctoral research fellow (PRF) grant award (about $100k per year for two years). Recently this PhD graduate accepted a full time position at Sandia National Lab. The one master degree graduate had already been employed by a materials related high tech company before her MS thesis defense in summer 2019. The project supported second PhD student (who is currently preparing his final PhD dissertation defense) has already been offered a full time job at a major high tech company while preparing his final PhD dissertation.

Results Dissemination: Over 21 publications and 18 presentations were documented during the project period. See section 8 "Result Dissemination" in the Final Progress Report.

Honors and Awards: During the project period, the project PI typically was awarded 1-2 faculty related honors/awards/certificates from the awardee organizational units every year, examples of the honors/awards/certificates include "Outstanding Researcher of the Year", "Outstanding Student Research Mentor of the Year", or "Outstanding Faculty Scholarship of the Year", etc. PI also won a research instrumentation award titled "Infrastructure Enhancement of Soft Materials Research/Education at NSU" (DOD Award # W911-NF-17-1-0450), and as a co-PI jointly won an NSF-CREST center grant award titled "CREST Center for Renewable Energy and Advanced Materials (CREAM)" (NSF Award # HRD-1547771). Most importantly, one of PI's PhD student mentees was voted as the outstanding PhD student awardee in 2018 at the awardee organization, and that same PhD graduate also successfully won a prestigious NSF postdoctoral research fellow (PRF) grant award (about $100k per year for two years).

Protocol Activity Status:

Technology Transfer: Nothing to Report

RPPR Final Report
as of 13-Jan-2020

PARTICIPANTS:

Participant Type: PD/PI
Participant: Sam Sun
Person Months Worked: 10.00 **Funding Support:**
Project Contribution:
International Collaboration:
International Travel:
National Academy Member: N
Other Collaborators:

BOOKS:

Publication Type: Book Peer Reviewed: Y **Publication Status:** 1-Published
Publication Identifier Type: ISBN Publication Identifier: 978-1-4665-8510-2
Book Edition: 2 Volume: Publication Year: 2017 Date Received: 31-Aug-2017
Publication Location: Florida, USA
Publisher: CRC Press
Book Title: Introduction to Organic Electronic and Optoelectronic Materials and Devices
Authors: Sam-Shajing Sun, Larry Dalton
Editor:
Acknowledged Federal Support: Y

CONFERENCE PAPERS:

Publication Type: Conference Paper or Presentation **Publication Status:** 1-Published
Conference Name: SPIE Optical Engineering + Applications
Date Received: 19-Aug-2016 Conference Date: 09-Aug-2015 Date Published:
Conference Location: San Diego, California, United States
Paper Title: Polymer light harvesting composites for optoelectronic applications
Authors: Sam-Shajing Sun, Dan Wang
Acknowledged Federal Support: **Y**

Publication Type: Conference Paper or Presentation **Publication Status:** 1-Published
Conference Name: SPIE Annual Convention
Date Received: 31-Aug-2017 Conference Date: 29-Aug-2016 Date Published: 29-Aug-2016
Conference Location: San Diego, California
Paper Title: Bridge Effects on Light Harvesting of a DBfA Type Polymer System
Authors: Sam-Shajing Sun, Muhammad Hasib, Alexander V. Gavrilenko, Joshua Devan, Vladimir Gavrilenko
Acknowledged Federal Support: **Y**

Publication Type: Conference Paper or Presentation **Publication Status:** 1-Published
Conference Name: Organic and Hybrid Sensors and Bioelectronics XI, SPIE
Date Received: 27-Aug-2018 Conference Date: 20-Aug-2018 Date Published: 20-Aug-2018
Conference Location: San Diego, California, USA
Paper Title: Polymer Composites for Potential Multi-Function Devices
Authors: Sam-Shajing Sun, Harold Lee
Acknowledged Federal Support: **Y**

RPPR Final Report
as of 13-Jan-2020

Publication Type: Conference Paper or Presentation **Publication Status:** 1-Published
Conference Name: SPIE International Conference
Date Received: 14-Nov-2019 Conference Date: 17-Aug-2019 Date Published: 31-Aug-2019
Conference Location: San Diego, CA
Paper Title: Polymer composites for potential thermo-electro dual sensors
Authors: Joseph Norman, Harold Lee, Sam Sun
Acknowledged Federal Support: **Y**

Publication Type: Conference Paper or Presentation **Publication Status:** 1-Published
Conference Name: SPIE Annual Convention
Date Received: 14-Nov-2019 Conference Date: 16-Aug-2019 Date Published: 10-Oct-2019
Conference Location: San Diego, CA
Paper Title: Block copolymer optoelectronic property versus bridge and morphology
Authors: Muhammad Hasib, Sam Sun
Acknowledged Federal Support: **Y**

DISSERTATIONS:

Publication Type: Thesis or Dissertation
Institution: Norfolk State University
Date Received: 27-Aug-2018 Completion Date: 7/13/18 11:57PM
Title: INVESTIGATION OF A SERIES OF DOPED P3HT COMPOSITES FOR THERMOELECTRIC AND PHOTOELECTRIC CONVERSIONS
Authors: Harold Lee
Acknowledged Federal Support: **Y**

Publication Type: Thesis or Dissertation
Institution: Norfolk State University
Date Received: 27-Aug-2018 Completion Date: 8/17/18 8:29PM
Title: INVESTIGATION OF A SERIES OF DOPED P3HT COMPOSITES FOR THERMOELECTRIC AND PHOTOELECTRIC CONVERSIONS
Authors: Harold Lee
Acknowledged Federal Support: **Y**

Publication Type: Thesis or Dissertation
Institution: Norfolk State University
Date Received: 14-Nov-2019 Completion Date: 7/30/19 9:15PM
Title: Synthesis and Properties of a Series of Metalized Octabutoxy-Phthalocyanine Dyes for Optoelectronic Applications
Authors: Stephanie Brookins
Acknowledged Federal Support: **Y**

PATENTS:

Intellectual Property Type: Patent Date Received:
Patent Title: Photoelectric and Thermoelectric Dual Conversion and Modulation Materials and Devices
Patent Abstract:
Patent Number: 62544857
Patent Country: USA

RPPR Final Report

as of 13-Jan-2020

Application Date: 13-Aug-2017 Application Status: 2

Date Issued:

Final Progress Report (FPR)

Project Title: Research and Education on Lightweight and Flexible Photo-/Thermo-Electric Multi-Functional Materials

Award/Grant Number: W911NF-15-1-0422

Period of Performance
Start: August 21 2015; **End:** August 20, 2019

Recipient of Grant
NORFOLK STATE UNIVERSITY
Norfolk, 23504-8060, USA

Principle Investigator
Dr. Sam Sun
Professor of Chemistry and Materials Science/Engineering

Report Date
November 18, 2019

Table of Contents

1. Progresses on Investigations of Thermoelectric/Photoelectric and Thermoelectric/Electroelectric Multi-Functional Materials

1.1 Proposed Research

One major or key research goal of the original proposal is to investigate and explore the possibility or feasibility of a photoelectric (PE)/thermoelectric (TE) dual-conversion material concept. **Figure 1.1** illustrate frontier orbital schemes of a donor/acceptor pair in (a) photoelectric doping; (b) chemoelectric doping; (c) thermoelectric doping; and (d) electro-electric doping processes [9]. These doping processes, if occurred, will generate or change corresponding mobile charge carrier densities.

Materials electrical conductivity (σ) is defined in equation (1.1) as

$$\sigma = en\mu \qquad (1.1)$$

where *e* is the charge of the particle, *n* is the mobile charge carrier density, and μ is the charge mobility. A material's thermoelectric Seebeck coefficient (α) is defined and can be experimentally measured via equation (1.2) (in units of μV/K) as

$$\alpha = -\Delta V/\Delta T \qquad (1.2)$$

The Seebeck coefficient is correlated to majority mobile charge carrier density *n* by equation (1.3) [3]:

$$\alpha = \frac{8\pi^2 {k_b}^2}{3eh^2} m^* T \left(\frac{\pi}{3n}\right)^{2/3} \qquad (1.3)$$

where k_b is the Boltzmann constant, *e* is the carrier charge, *h* is Planck's constant, *m** is the effective mass of the majority mobile charge carrier, and *n* is the majority mobile charge carrier density. In our study, carrier density *n* is directly related to the photoelectric or thermoelectric doping induced positive polarons on P3HT, and that the carrier mobility μ is generally and directly correlated to materials solid state packing or film morphology. If the solid state packing or film morphology are the same or similar (such as within a narrow range of temperature change), then the conductivity can reflect doping induced carrier density changes.

To demonstrate a PE/TE dual conversion material, as an example, a conjugated p-type polymer such as P3HT doped with both a photoelectric acceptor dopant (acceptor-P) and a thermoelectric acceptor dopant (acceptor-T), or a ternary composite materials system based on their frontier orbital levels and offsets are illustrated in **Figure 1.2**. Chemical structures of some representative candidate/example materials and their frontier orbital levels are shown in **Figures 1.3** and **Figure 1.4**. Thermoelectric properties including Seebek coefficients (α) and thermoelectric power factor ($\alpha^2\sigma$), as well as electrical conductivity (σ) versus charge carrier concentrations are shown in **Figure 1.5**. It is clear charge carrier density can effectively affect or modulate the materials thermoelectric properties.

Parameters that would affect either PE or TE conversions will be systematically studied in the proposed research, these include, but may not limited to, frontier orbital levels and off sets, doping ratios of the three components, molecular structure and solution processability, solid state morphologies, temperature, and radiation intensity. The research objective is to identify a parameter set or condition where both photoelectric and thermoelectric conversions would work efficiently at the same time for the same composite, and that one conversion can modulate the other conversion effectively. Scientific outcome or impact of this research include, but may not limited to, fundamental knowledge on such photoelectric/thermoelectric dual-conversion material and devices.

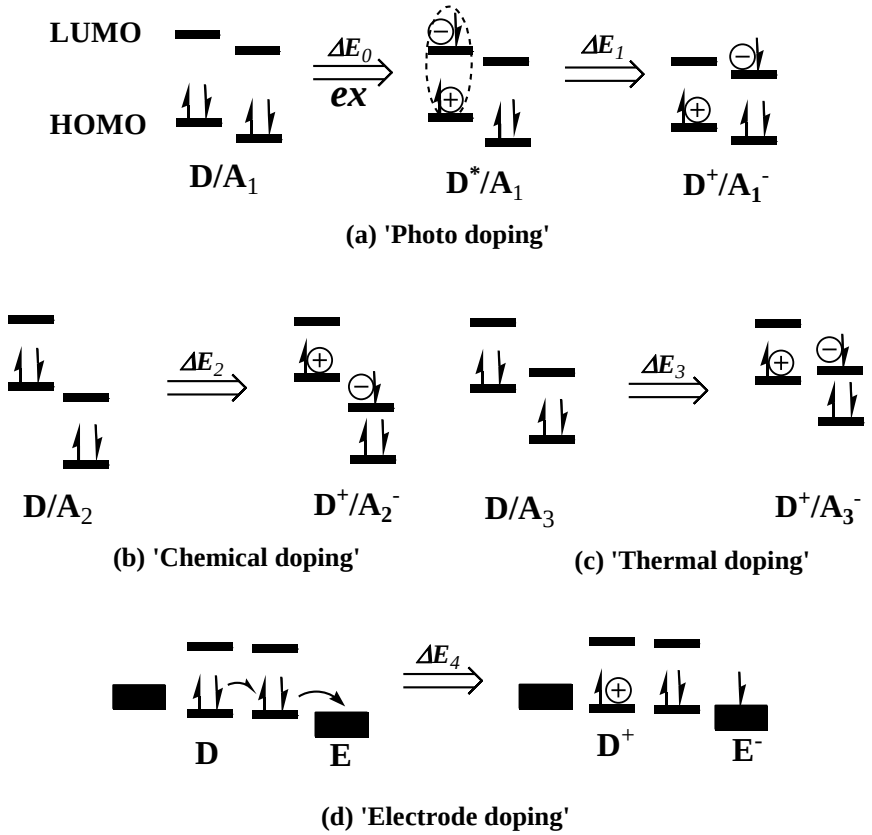

FIGURE 1.1 Scheme of frontier orbitals and electron transfers of (a) photoelectric doping; (b) chemoelectric doping; (c) thermoelectric doping; and (d) electroelectric doping processes [9].

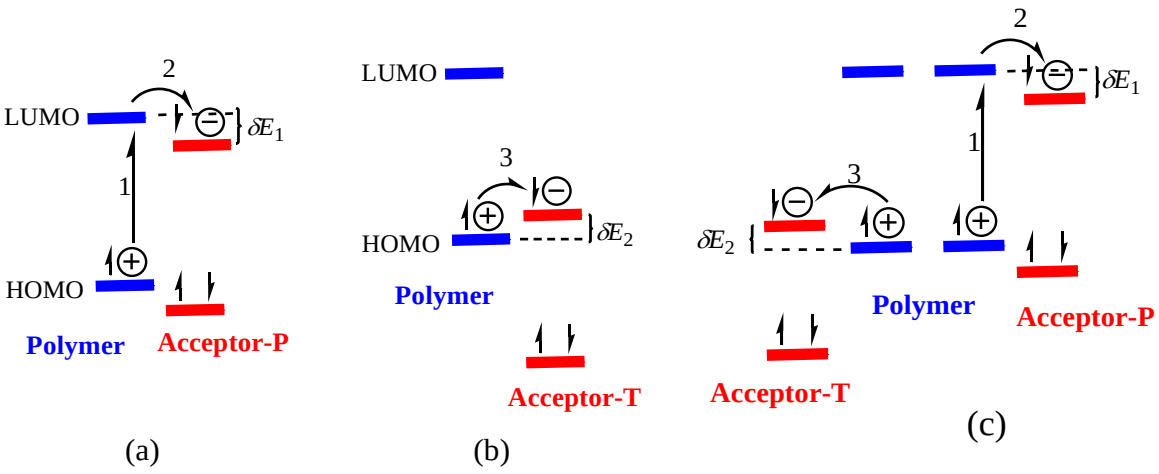

Figure 1.2 Molecular frontier orbital schemes of (a) photo doping (for photo-electric or PE conversions); and (b) thermal doping (for thermoelectric or TE conversions), and (c) novel thermo-photo-electro TE/PE dual-conversion systems.

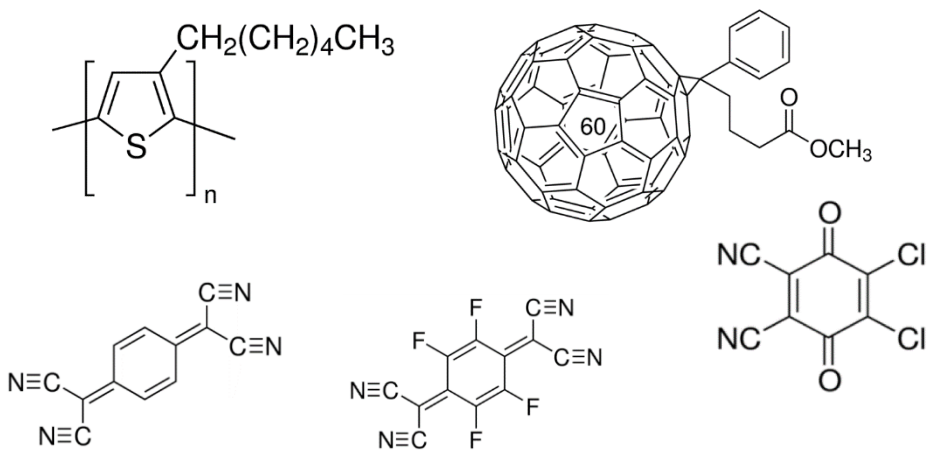

Figure 1.3 Chemical/molecular structures of example/candidate materials P3HT (top left, an example/candidate donor or P type of conjugated polymer), $PC_{60}BM$ (top right, an example/candidate photo acceptor or Acceptor-P), TCNQ (bottom left, an example/candidate thermal acceptor or Acceptor-T), and F4-TCNQ (bottom middle, an example/candidate thermal acceptor or Acceptor-T), and DDQ (bottom right, an example/candidate thermal acceptor or Acceptor-T).

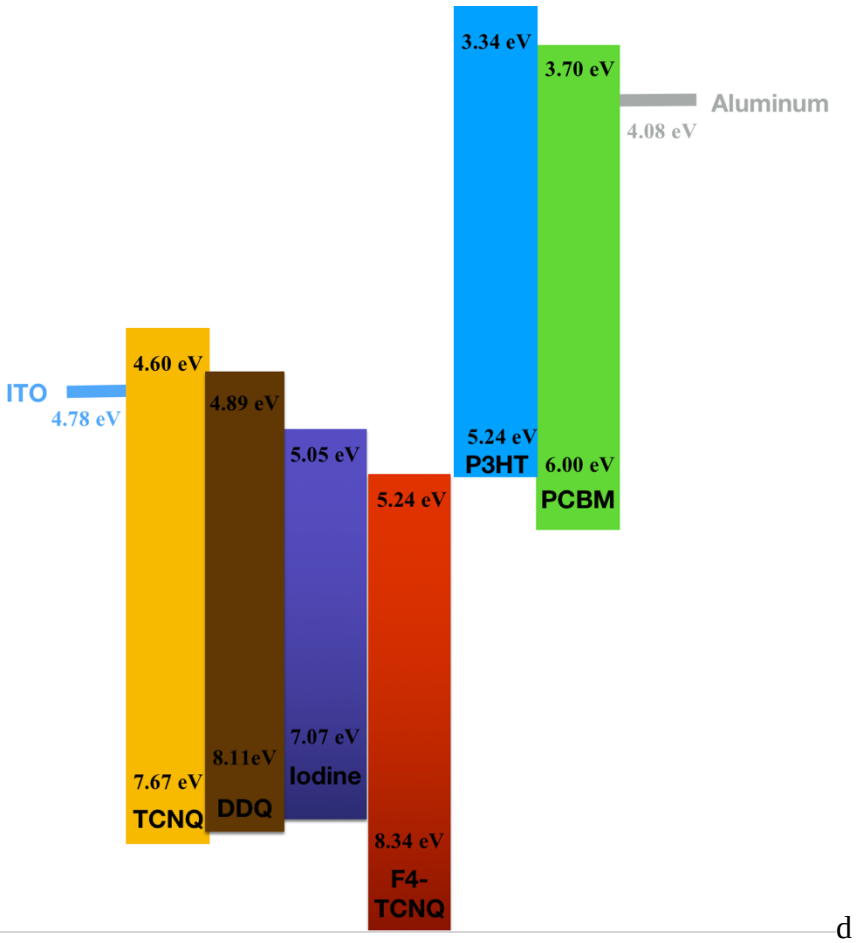

Figure 1.4 HOMO/LUMO levels of candidate/example materials.

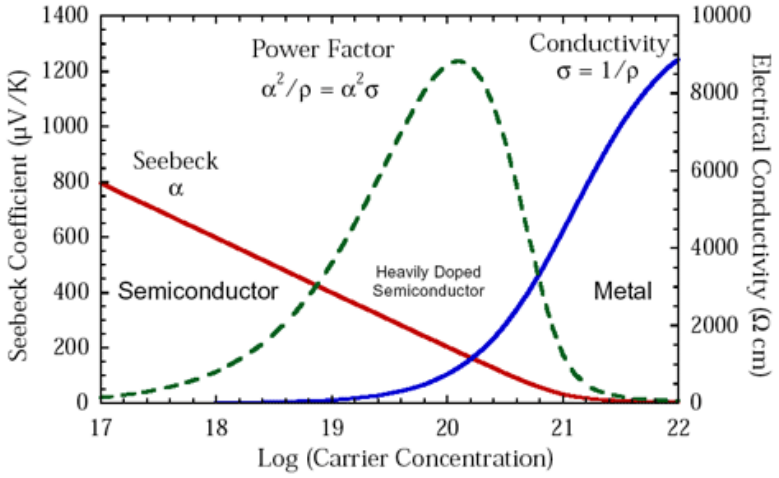

Figure 1.5 Scheme of thermoelectric Seebeck coefficient (α), thermoelectric power factor *TPF* ($\alpha^2\sigma$), and electrical conductivity (σ) versus charge carrier concentrations.

1.2 Demonstration of Photoelectric (PE)/Thermoelectric (TE) Dual Conversion and Dual Modulation Via A Ternary Composite

In order to test a PE/TE dual conversion concept or feasibility, a popular PE polymer pair P3HT:$PC_{60}BM$ coupled with a thermoelectric acceptor dopant (such as iodine, see **Figures 1.3-4**) were investigated first [27-28, 33]. In a ternary P3HT:$PC_{60}BM$:Iodine system, the p-type polymer is P3HT, the "Acceptor-P" is $PC_{60}BM$, and the "Acceptor-T" is iodine.

Experimental

P3HT (Product #:698997), PCBM (Product #:684430), 7,7,8,8-tetracyanoquinodimethane received from Sigma-Aldrich without further purification. 1,2-dichlorobenzene (Product #:A13881) and iodine (Product #:A12278) were used as received from Alfa Aesar without further purification. This resulted in a molecular system with the highest occupied molecular orbital (HOMO) and lowest unoccupied molecular orbital (LUMO) values of each material and the frontier orbital offsets creating a desired ternary composite shown in **Figures 1.3-4**.

As an example, a P3HT stock solution was made by dissolving 30 mg of P3HT into 2 mL of 1,2-dichlorobenzene resulting in a solution concentration of 15:1 mL of P3HT:1,2-dichlorobenzene. Iodine doping was carried out at a mole ratio of 5% with respect to P3HT repeat units. The mass for 5% mole ratio of iodine was weighed into an individual vial. A 1 mL aliquot of the stock solution was then placed into the vial containing the iodine. This resulted in two solutions; pure P3HT and 5% iodine doped P3HT solutions. Similarly, a stock P3HT:PCBM solution was made by dissolving 30 mg of P3HT and 30 mg of PCBM (equal weights) into 2 mL of 1,2-dichlorobenzene resulting in a solution concentration of 15:15:1 mL of P3HT:PCBM:1,2-dichlorobenzene. The mass for 5% mole ratio of iodine (compared to P3HT repeat units) was weighed into an individual vial. A 1 mL aliquot of the P3HT:PCBM stock solution was then placed into the vial containing iodine. This resulted in two solutions; pure P3HT:PCBM composite and 5% iodine doped P3HT:PCBM composite solutions, also called Iodine:P3HT:PCBM ternary composite. Thin films were prepared by spin coating previously prepared solutions on ITO coated glass slides (for OPV devices) or silicon wafer strips (for TE analysis). Glass slides were sonicated in DI water, acetone, and isopropanol for five minutes each and then plasma cleaned in oxygen for 15 minutes. ITO coated glass slides for device fabrication were made by etching away ITO from the outside edges of the slide using 6M hydrochloric acid leaving a strip of ITO in the center of the slide. The slides were then cleaned similar to plain glass slides minus the oxygen plasma cleaning. Solutions were then spin coated at 1000 rpm for 180 seconds. Thin films were then transferred in a vacuum oven and dried at 80˚C overnight (~17 hours) under -30 mmHg vacuum. It is important to note that films were dried individually, not all together, to prevent any cross contamination between doped samples. Devices were made by evaporating aluminum contacts through a shadow mask under $2x\ 10^{-6}$ mbar vacuum in a thermal evaporator inside of an MBraun Glovebox. Devices were constructed using the standard OPV device structure. Bottom electrode was ITO and the top contact was

aluminum. For solar cell studies, the entire thin film OPV slide was irradiated by an Oriel 1kW solar simulator at half Sun intensity (50 mW/cm^2). Each cell device had an area of 0.25 cm^2 was illuminated in an inert environment. TE sample illumination studies utilized various light intensities of a E363178 LED Desk Lamp (Model MTSL1001AYS-LED3.5k840). TE measurements were conducted using a MMR SB1000 Digital Seebeck Controller at room temperature with a 132 gauge constantan wire as a reference, and with a heater power up to 250 mW, and with a 30 second initial and operation delay.

Results and discussion

In order to demonstrate PE/TE dual-conversions, the photoelecctric and thermoelectric induced electrical conductivities need to be measured first under either heating or light illuminations or both. Specifically, the dual conversion and dual modulation can be demonstrated via a thermally-modulated solar cell and light-modulated thermoelectric Seebeck coefficients.

Prior to device fabrications and evaluations, thin film electrical conductivities were measured for pristine P3HT and 5% iodine doped P3HT films (**Figure 1.6**) and for P3HT:PCBM:Iodine ternary films (**Figure 1.7**) under four different conditions:

A. Room temperature in the dark (RT, 25˚C),
B. Heated to an elevated temperature in the dark (ET, 39˚C),
C. Room temperature and under a 50 mW/cm^2 AM 1.5 solar simulator illumination (RT + Light) and
D. Heated to the elevated temperature and under a 50 mW/cm^2 AM 1.5 solar simulator illumination (ET + Light)

Temperature changes were limited to a very narrow range (about 14^{o}C) in order to eliminate or mitigate the effects of changes in morphology upon heating of P3HT and its composites. As seen in **Figure 1.6**, pristine P3HT conductivity remains relatively stable or unchanged upon either heating or light radiation. For the 5% iodine doped P3HT sample, however, the P3HT conductivity exhibited a dramatic increase upon temperature increase, and it was believed to be due to the thermoelectrically-induced free holes in P3HT upon heating. With the addition of PCBM as in the ternary P3HT:PCBM:Iodine, as seen in **Figure 1.7**, upon illumination, dramatic increases in conductivity were also observed due to photo doping process of P3HT:PCBM, *i.e.*, both TE and PE processes can occur symultaneously.

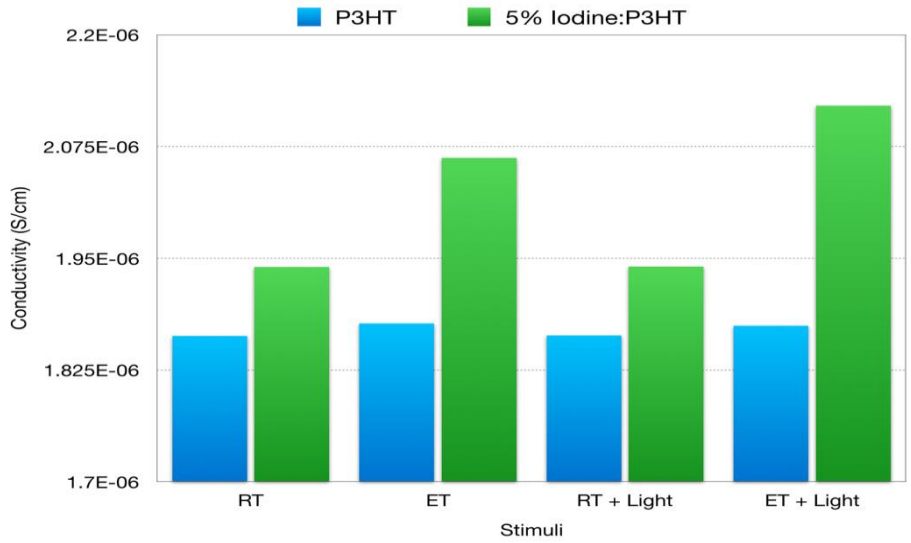

Figure 1.6 Electrical conductivity of pure P3HT and 5% iodine doped P3HT thin film samples measured at room temperature (RT, 25^{o}C), elevated temperature (ET, 39^{o}C), room temperature under light illumination, and elevated temperature under light illumination.

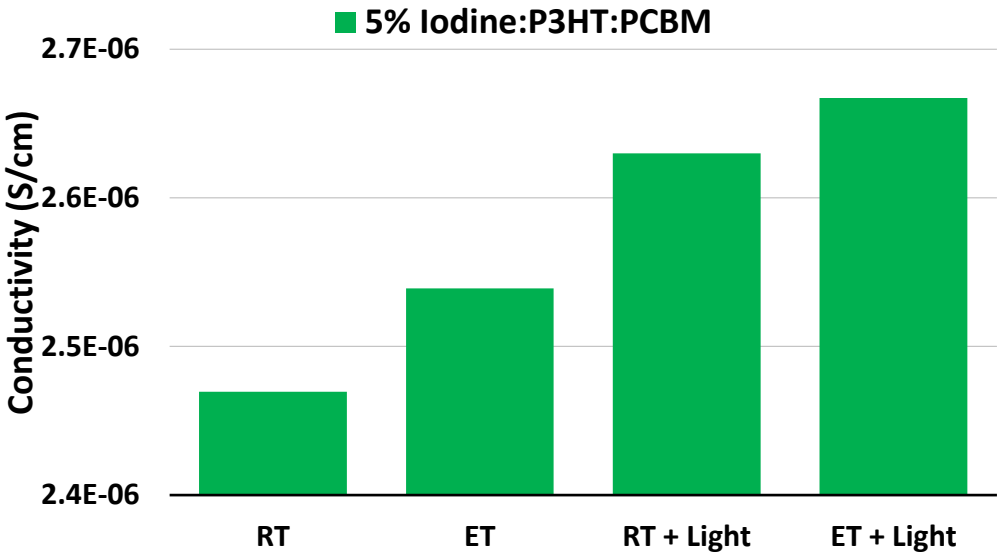

Figure 1.7 Electrical conductivities of 5% iodine doped P3HT:PCBM at room temperature (RT**,** 25^{o}C), elevated temperature (RT**,** 39^{o}C), room temperature under illumination, and elevated temperature under illumination [27-28, 33].

TEMPERATURE MODULATION OF PHOTOELECTRIC CONVERSIONS

In literature, an ambient temperature iodone doped P3HT:PCBM cell was studied for solar cell [1] and for infred photo detector applications [2]. In this study, the solar cell or photo detector photo I-V curves and overall power conversion efficiencies (PCE) were

systematically evaluated at different temperatures in order to evaluate thermoelectric conversion effects toward photoelectric conversions. **Figure 1.8** present the photoelectric I-V curves of 5% iodine doped P3HT:PCBM solar cells at room temperature and when heated. **Tables 1.1** list the data used to calculate the PCE of 5% iodine doped P3HT:PCBM solar cells at the same two different temperatures respectively.

As illustrated in **Figure 1.8** and **Table 1.1**, significant increases in all factors such as V_{oc}, I_{sc} and an overall 22% increase in the PCE as were observed upon heating. On the other hand, the P3HT:PCBM cell without iodine doping did not exhibit any non-negligible changes upon heating. Thus, thermoelectric modulation of the the photoelectric conversion was confirmed and demonstrated.

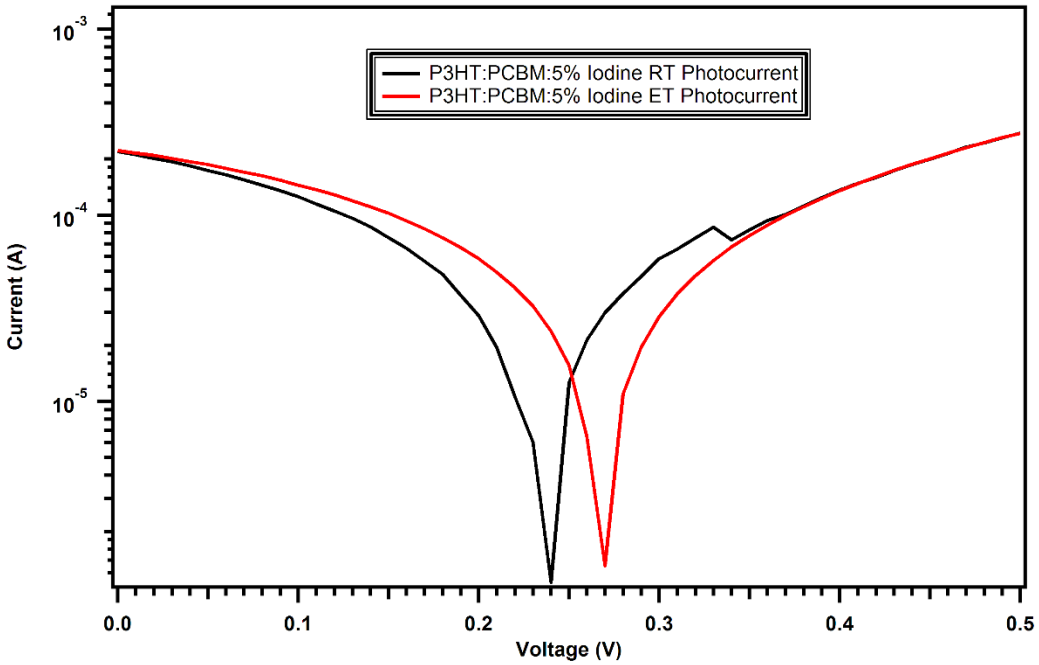

Figure 1.8 Temperature modulation of photoelectric I-V curves of P3HT:PCBM:iodine ternary thin films at room temperature (25^{o}C, left black curve) and at an elevated temperature (39^{o}C, right red curve).

Table 1.1 PCE values of a 5% iodine doped P3HT:PCBM device at room temperature (25°C) and when heated to an elevated temperature (39°C).

5% I_2:P3HT:PCBM	Room Temperature	Elevated Temperature
Cell Area (cm^2)	0.25	0.25
I_{sc} (mA)	0.220	0.222
V_{oc} (mV)	235	265
I_{pmax} (mA)	0.105	0.119
V_{pmax} (mV)	120	130
Fill Factor	0.24	0.26
P_{in} (mW/cm^2)	49.8	49.8
Raw PCE	0.254	0.312
Corrected PCE	0.045	0.051
	% Increase	22.8

LIGHT MODULATION OF THERMOELECTRIC CONVERSIONS

The key thermoelectric parameters of study here is the Seebeck coefficient as expressed in **Equations 1.2** and **1.3**. As **equation (1.2)** shows, the sign of the measured Seebeck coefficient indicates the majority carrier in the system, meaning positive Seebeck coefficient indicates a p-type material and vice versa. The Seebeck coefficient can be further expanded into **Equation 1.3**, where it provides insight on how charge carrier densities *n* would affect Seebeck coefficient. In our case, the Seebeck coefficients is modulated via light. Photo-Seebeck effects were reported in certain inorganic semiconductors and metal oxides such as ZnO, PbO, ZnS, Cu_2S, etc [4-7]. The photo-Seebeck effect was referred to as the thermoelectric transport of photo-induced carriers in a material. The criteria for a material to exhibit such effects are not yet clear even in most inorganic materials.

To illustrate the dual conversion and dual modulation effects, the Seebeck coefficients of pure P3HT, P3HT doped with iodine, P3HT photo-doped with PCBM, and P3HT doped with both PCBM and iodine were all evaluated. The conductivities as well as Seebeck coefficients were studied with and without heat or light illuminations. Without the presence of a photo acceptor-P such as PCBM, upon illumination (LED Desk Lamp E363178, 120V, 60Hz, 3.5W, 0.035A. Lamp Model: MTSL 1001AYS-LED3.5L840), both conductivities and Seebeck coefficient remain relatively the same. However, as shown in **Figure 1.9**, the thermoelectric Seebeck coefficients of Iodine/P3HT/PCBM ternary composite thin films (bottom red curve) under dark and under different light illumination intensities up to about 20 mW/cm^2 (same LED lamp described above) exhibited initial increase then decreases at an intensity of about 8 mW/cm^2. A P3HT/PCBM binary composite film (top black curve) was also measured for comparison. The Seebeck coefficients of the binary film is higher than the ternary film due to ternary composite film has higher hole densities as a result of iodine doping. In both cases, the

initial increase of Seebeck coefficient versus light intensity from dark to about 8 mW/cm^2 may be attributed to an electron-photon coupling mechanism where the Seebeck coefficients were dominated by an increasing effective mass of the mobile charge carriers at low light intensity or low charge density regime [8], and the decrease of the Seebeck coefficient passing the 8 mW/cm^2 can be accounted by a dominant Seebeck versus mobile carrier density relationship as expressed in equation (1.3) [3].

These experimental results and data clearly demonstrate that light can be used to effectively modulate the thermoelectric conversion of a material if the material is doped with both a photoelectric dopant as well as a thermoelectric dopant with appropriate frontier orbital level relationship. In this demonstration, the change of thermoelectric Seebeck coefficients between dark and highest photo modulated Seebeck is about 10% [28]. With further and systematic studies and optimizations, it is possible that light could more effectively modulate the thermoelectric conversion of the material.

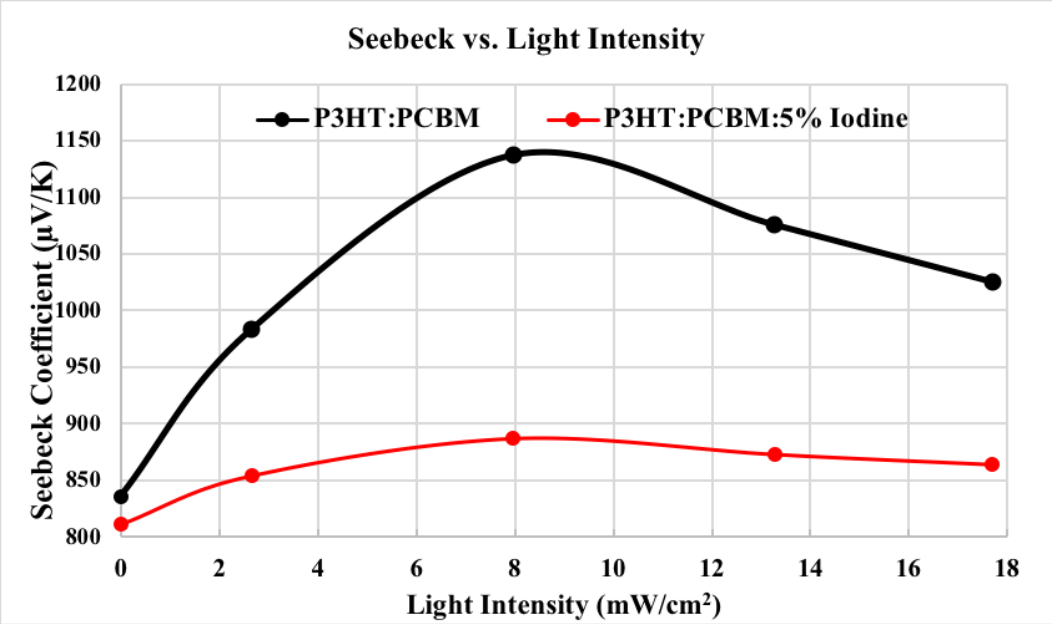

Figure 1.9 Light modulation of themoelectric Seebeck coefficients of a binary P3HT:PCBM (top curve) and a ternary P3HT/PCBM/iodine (bottom curve) films in the dark and under different light intensities of an LED lamp [28, 33].

1.3 Demonstration of Thermoelectric/Electroelectric Dual Conversion and Dual Modulation Via A Binary Composite

Sample Preparation: Regio-regular P3HT (Rieke Metals via Aldrich SKU 445703) and iodine (Alfa Aesar SKU 00158) were used as purchased without further purification. P3HT was placed into a nitrogen glovebox prior to being opened from the supplier and was dissoluted in 1,2-dichlorobenzene (Merck SKU 8:03238.1000) at a concentration of 8 mg/mL then stirred overnight. Iodine was weighed at previously calculated dopant concentrations from 0.1% and 1% mole ratio into separate vials in atmosphere then the vials were transferred to a nitrogen environment where the stock P3HT solution was added. Those solutions were then stirred overnight. If any remaining undissolved P3HT on Iodine was observed, samples were lightly heated for approximately 10 minutes while stirring before storing them in the nitrogen environment.

Thin Film Device Fabrication and Characterization: OFETs were fabricated using heavily-doped n-type Si wafers with a 300 nm dry thermal oxide to function as the gate dielectric by D&X Co. Diced individual samples were cleaned in ultrasonic bath by a sequence of acetone and isopropanol for 30 minutes each and followed by drying with a stream of forced nitrogen. Specimens were then plasma-cleaned in oxygen for 15 minutes. The SiO_2 was then surface modified with octadecyltrichlorosilane (OTS) by immersion in a 10 mM solution at approximately 60 °C for 20 minutes then rinsed in an ultrasonic bath with chloroform for 10 minutes. Source, drain, and gate contacts consisting of a 5 nm Cr adhesion layer and a 60 nm Au layer were then deposited via thermal evaporation. Samples were then plasma-cleaned in oxygen for 30 s immediately before spin-coating of the semiconductor layer. Spin-coating was accomplished in nitrogen environment by applying 80 µL of solution via micropipette to the surface of the bottom gate bottom contact (BGBC) substrates and spinning at 1500 rpm for 120 s. The samples were then removed from the nitrogen environment where undoped and doped devices were placed in separate vacuum ovens and dried in vacuum at 120°C for 20 minutes. Electrical contact areas for characterization were cleaned with a chloroform-dipped foam swab and independent devices were isolated with a fine razor under magnification before being placed into a nitrogen glovebox for storage. Devices were held in the nitrogen and moisture-controlled environment until removed for characterization in atmosphere. Samples for XRD evaluation were prepared on the same substrates as OFETs, with the exception of the thermal evaporation step and stored in the same manner.

Output and transfer curves were obtained on a Signatone probe station in air under ambient conditions. Samples were placed on a Tetech plate cooler controlled with a TE-720 temperature control module. A small amount of heat sink grease was placed between the sample and the plate cooler to facilitate uniform heating and cooling of the DUT. Surface temperatures were verified with a FLIR camera and samples were allowed to equilibrate prior to electrical characterization.

Thermoelectric Temperature Modulation of FET

Figure 1.10 exhibits output source-drain IV curves for 0.1% iodine-doped P3HT thin film FET devices with a channel length of 60 µm and a channel width of 1000 µm. Devices were tested with surface temperatures at three different temperatures of 17.5ºC, 21ºC and 24ºC. **Figure 1.11** exhibits the transfer curves of the same FET devices at the same temperatures. The temperature modulation of FET devices are demonstrated [29].

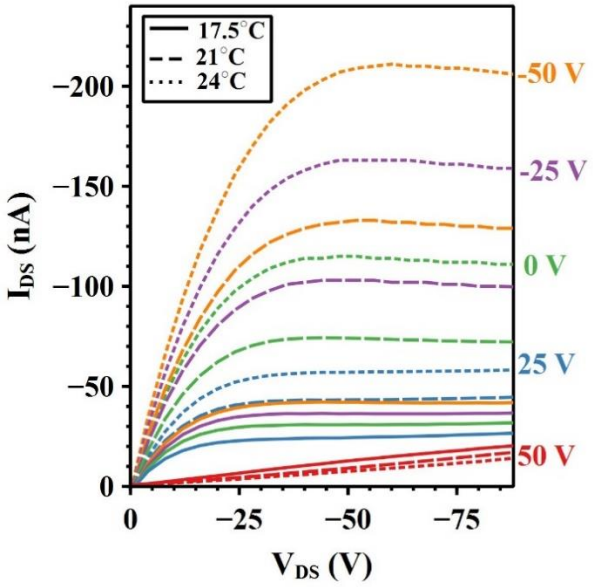

Figure 1.10 Temperature modulation of IV_{SD} curves of 0.1% iodine doped P3HT FET devices

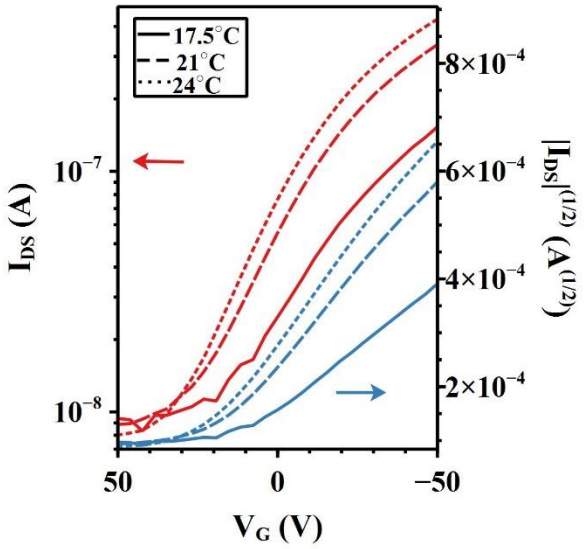

Figure 1.11 Temperature modulation of transfer curves of a 0.1% iodine doped P3HT FET devices.

Gate Voltage Modulation of Thermoelectric Seebeck Coefficients

Figure 1.12 exhibits gate voltage modulation of the thermoelectric Seebeck coefficients of 0.1% iodine doped P3HT thin film FET devices. As the data show, with increase of positive gate voltage (or decrease of hole density as P3HT is a p-type semiconductor), the Seebeck coefficients should increase (as expected from **Figure 1.5)**. The experimental data demonstrates that gate voltage can indeed effectively modulate the thermoelectric properties of the thin films. Additional studies are going on to optimize such function.

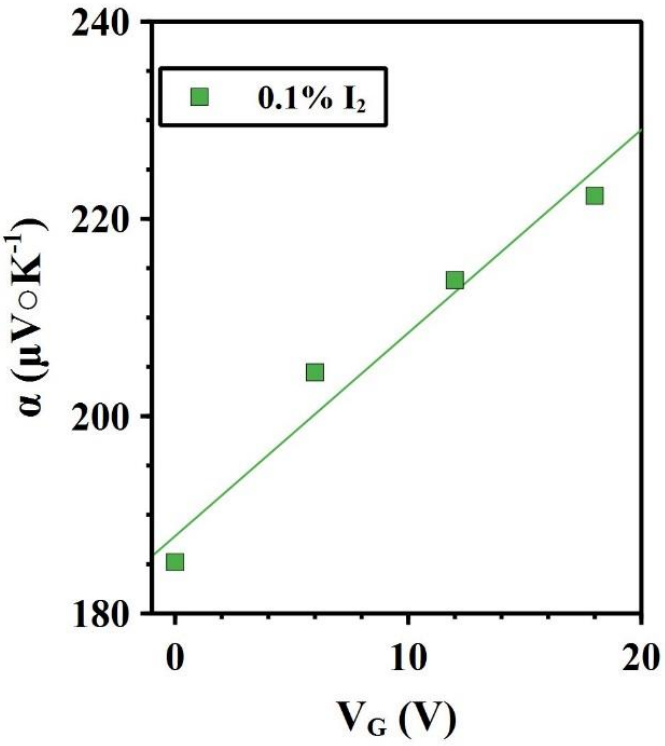

Figure 1.12 Gate voltage modulation of thermoelectric Seebeck coefficients of iodine doped P3HT thin film FET devices.

SUMMARY AND CONCLUSIONS

Our preliminary experimental results clearly demonstrated the feasibility or potential of a photoelectric/thermoelectric and a thermoelectric/electro-electric dual conversion modulator/switching materials and devices based on a binary iodine doped P3HT and a ternary iodine doped P3HT:PCBM composites. However, materials, processing, fabrications, and device parameters should be further systematically investigated and optimized in order to fit a particular application need.

1.4 Correlation of Frontier Orbital Levels, Offsets, and Properties of A Series Thermoelectric Acceptor Doped P3HT and P3HT:PCBM Composites

Introduction

To achieve p-type thermoelectric doping of organic semiconductors, dopant molecule's LUMO should be close to the HOMO of the host material [9]. The orbital offset between the dopant LUMO and host HOMO facilitate electron transfer from the host material (donor) to the dopant molecule (acceptor). For a conjugated polymer host, once this electron transfer occurs, positive charges are formed on the donor polymer causing localized structural distortion that could result in changings from benzoid to quinoid structure change in the conjugated backbone along with the formation of polarons and/or bipolarons. When chemical doping is done in solution, the charge transfer can lead to aggregation of the host polymer due to the formation of either charge-transfer complexes or ion-pair formations. These aggregates result in drastic changes in the overall thin film morphology and related properties [10]. Another critical area to address is the optimum dopant for a particularly polymer. We believe this is directly related to the frontier orbital offsets between the polymer and the acceptor-T which is a key electron transfer driving force and it may follow Marcus electron transfer model. It is well known that in some organic semiconductors such as P3HT, the electrical conductivity versus different dopant is not a linear relationship. For example, when P3HT is doped with F4-TCNQ, as the dopant concentration is increased, a decrease in conductivity is observed at ultra-low and ultra-high doping levels followed by a linear and nonlinear increase at moderate doping levels, which is attributed to filling of electronic trap states [11]. To determine the role acceptor strength has in the thermoelectric doping process, the effects of varying dopant-T such as TCNQ, DDQ, iodine, and F4-TCNQ with P3HT and P3HT:PCBM composite solutions and thin films are being evaluated (See **Figures 1.3-4**). All acceptor-T are doped at 5% mole ratio to P3HT repeat unit. Our results indicate F4-TCNQ (the strongest acceptor) oxidizes P3HT the most, while TCNQ (the weakest acceptor) has negligible effects on the optoelectronic and thermoelectric properties of P3HT and its composites.

Materials and method

P3HT (Product #:698997), PCBM (Product #:684430), 7,7,8,8-tetracyanoquinodimethane (TCNQ) (Product #:157635), and 2,3-dichloro-5,6-dicyano-p-benzoquinone (DDQ) were used as received from Sigma-Aldrich without further purification. 1,2-dichlorobenzene (Product #:A13881) and iodine (Product #:A12278) were used as received from Alfa Aesar without further purification. Tetrafluorotetracyanoquinodimethane (F4-TCNQ) was used as received from TCI Chemicals (Product #:T1131) without further purification. Chemical structures of these materials are shown in **Figure 1.3**. The highest occupied molecular orbital (HOMO) and lowest unoccupied molecular orbital (LUMO) values of each material and the frontier orbital offsets are displayed in **Figure 1.4**.

A stock P3HT solution was made by dissolving 60 mg of P3HT into 4 mL of 1,2-dichlorobenzene resulting in a solution concentration of 15:1 mL of P3HT:1,2-

dichlorobenzene. All acceptor-T solution doping was prepared at a mole ratio of 5% with respect to P3HT. The mass for 5% mole ratio of each dopant was weighed into individual vials. 1 mL aliquots of the stock solution were then placed into each vial containing the different amounts of each dopants. This resulted in solutions ranging from weak to strong acceptor doped P3HT solutions. A stock P3HT:PCBM solution was also made by dissolving 60 mg of P3HT and 60 mg of PCBM into 4 mL of 1,2-dichlorobenzene resulting in a solution concentration of 15:15:1 mL of P3HT:PCBM:1,2-dichlorobenzene and subsequently doped by different acceptor-T in the same way as described above.

Thin films were prepared by spin coating previously prepared solutions onto plain glass slides. Glass slides were tripled sonicated in DI water, acetone, and isopropanol for five minutes each and then plasma cleaned in oxygen for 15 minutes. ITO coated glass slides for device fabrication were made by etching away ITO from the outside edges of the slide using 6M hydrochloric acid leaving a strip of ITO in the center of the slide. The slides were then cleaned similar to plain glass slides minus the oxygen plasma cleaning. Solutions were then spin coated at 1000 rpm for 180 seconds. Thin films were then transferred in a vacuum oven and dried at 80˚C overnight (~17 hours) under -30 mmHg vacuum. It is important to note that films were dried individually, not all together, to prevent any cross contamination between doped samples. Devices were made by evaporating aluminum contacts through a shadow mask under 2x 10^{-6} mbar vacuum in a thermal evaporator inside of an MBraun Glovebox. Device was constructed using the standard OPV device structure. Bottom electrode was Indium Tin Oxide and the top contact was aluminum. The entire thin film is irradiated by the solar simulator. Each device had an area of 0.25 cm^2

Dynamic Light Scattering (**Figure 1.14**) was conducted using a Microtrac Nanatrac Wave II. UV/Vis spectroscopy was conducted using a Perkin Elmer UV/Vis/NIR Spectrometer Lambda 1050 using the 60 mm InGaAs integrating sphere either in solution inside quartz vials or as thin films. Photoluminescence of the solutions were conducted using a Jobin-Yvon/Horiba Fluoromax-3 with an excitation wavelength of 465bP3HT:PCBM solutions. Atomic force microscopy (AFM) images were collected using a Digital Instruments Dimension 3100 in tapping mode with a scan area set at 5 µm x 5 µm. AFM data analysis was conducted using a Nanoscope Analysis version 1.40 by Bruker. X-ray diffraction was conducted using a Phillips Panalytical X'Pert MRD X-ray diffractometer using a Cu Kα source (λ = 1.5406 Å). Polymer film thicknesses were measured with a Dektak-6M profilometer.

Polymer solar cell devices were fabricated and tested inside a custom built MBraum inert gas glove box system coupled with an electrode vacuum thermal deposition chamber (vacuum up to 1 x 10^{-7} mbar), a solar simulator (providing a one-Sun or 100mW/cm^2, 1.5 AM simulated sunlight radiation), and a current-voltage source-measure-unit (Keithley SMU-237), and a data processing PC. For our conductivity studies, films were illuminated under 0.5 Sun (or 50 mW/cm^2 1.5 AM simulated sunlight radiation) from an Oriel I kW Solar Simulator.

Results and discussion

In solution, the acceptor-T doped P3HT:PCBM composites generated suspension particles that became more evident as stronger acceptors were used. For instance, a color change and a change in solution viscosity was observed as acceptor strength was increased. To better characterize this aggregation effect, dynamic light scattering (DLS) studies that are sensitive to aggregate or particle sizes in solution were measured. **Figure 1.14** exhibits the DLS spectra of P3HT dichlorobenzene (DCB) solutions doped with various acceptors. The solution polymer aggregate particle sizes are growing versus acceptor strength. Pure P3HT has very small particles mainly attributed to the polymer chains themselves while very little self-aggregation may occur as seen in the DLS with a small amount of particles between 10-100 nm. TCNQ, which is a weak acceptor, has little effect on aggregation as seen in the solution phase and is similar to 1% iodine doping of P3HT. Lüssem *et. al*. reports that at lower iodine doping concentrations, doped films of P3HT resemble the structure or morphology of undoped films of P3HT and this may be due to low oxidation or no doping at all [12]. For acceptors with strength higher than that of TCNQ, we begin to see more dopant induced aggregation.

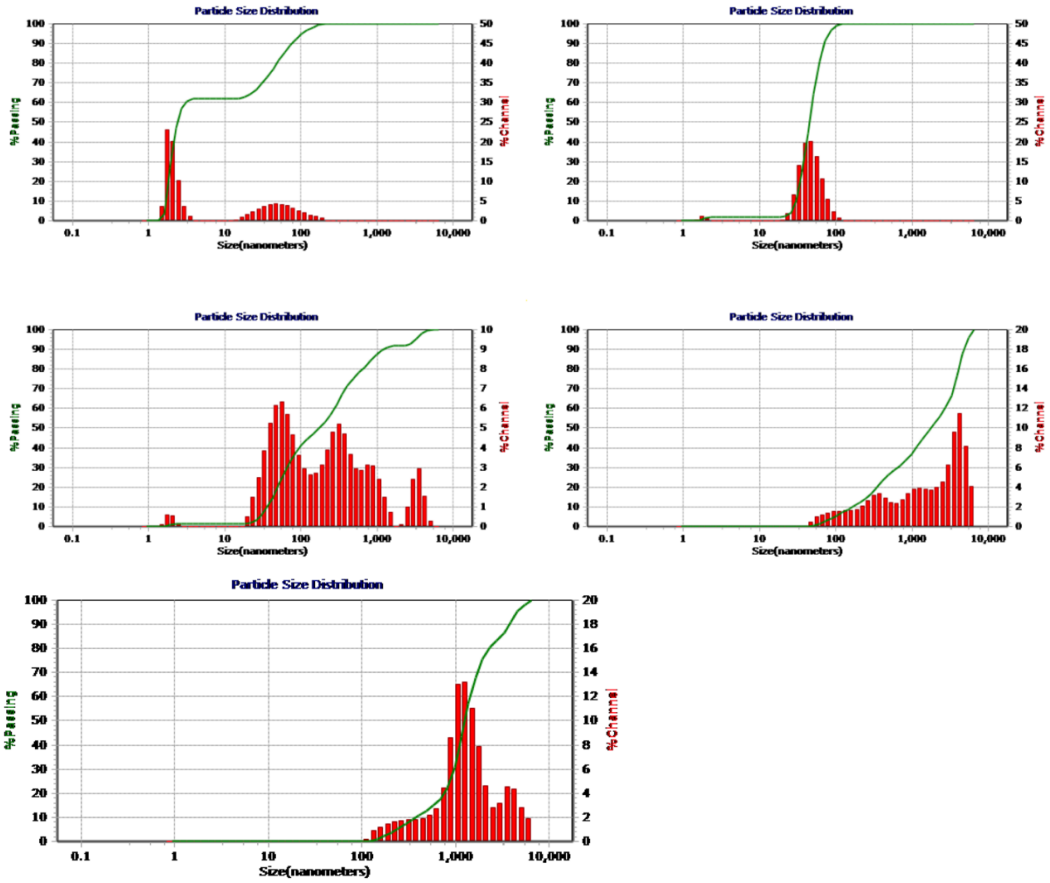

Figure 1.14 Dynamic Light Scattering (DLS) spectra of P3HT in dichlorobenzene (DCB) solutions of pure P3HT (top left), 5% TCNQ doped (top right), 5% DDQ doped (middle left), 5% I_2 doped (middle right), and 5% F4-TCNQ doped (bottom).

UV/Vis absorption and photoluminescence (PL) spectra were measured for acceptor-T undoped and doped P3HT and P3HT:PCBM composites in dichlorobenzene (DCB) solution and thin film states. In the solution state, both pristine P3HT and P3HT:PCBM blend solutions were evaluated. **Figures 1.15-16** exhibit the UV/Vis and PL spectra of pristine P3HT dichlorobenzene (DCB) solutions doped with various acceptors. In the UV/Vis, as the acceptor strength increases from TCNQ, to DDQ, to iodine, and finally to F4-TCNQ, the main absorption peak at about 470 nm decreases while aggregation and/or polaron peaks at over 600 nm wavelength increases.

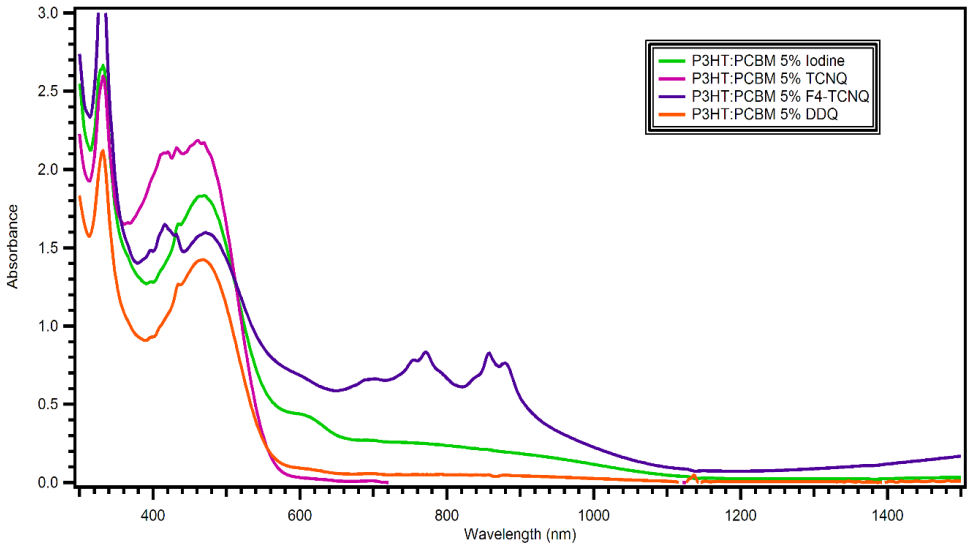

Figure 1.15 UV/Vis absorption spectra of P3HT:PCBM composite solutions doped with various acceptors.

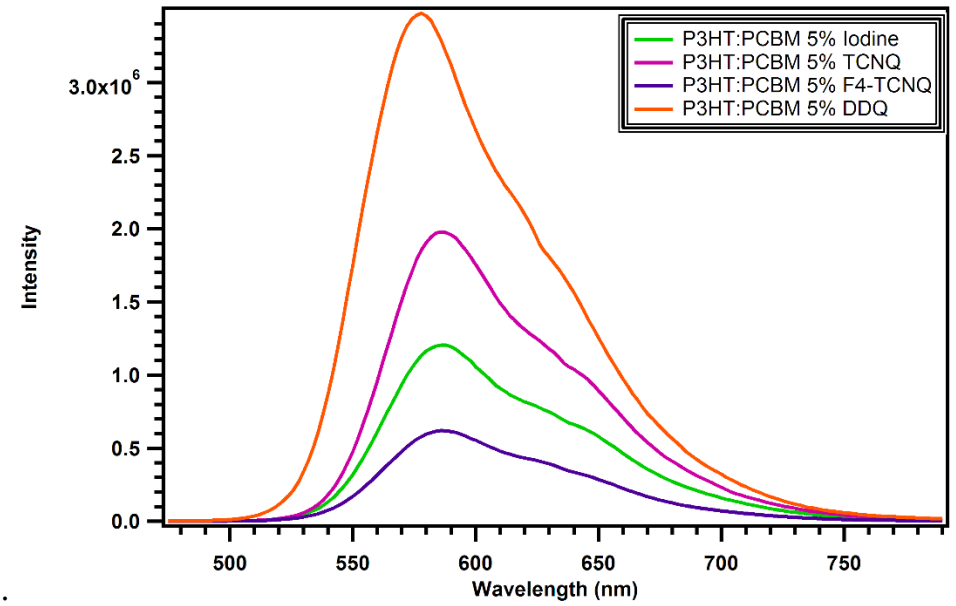

Figure 1.16 PL emission spectra of P3HT:PCBM composite solutions doped with various acceptors.

The main UV-Vis absorption peak (470 nm) decease indicates reduction of the neutral state of P3HT and the formation of the aggregated or the doped states. Dopant molecules act as electron acceptors or traps with respect to polymer. As a result, new optical transitions arise at lower energies than the neutral polymer state. Note that pristine or pure conjugated polymers do not contain intrinsic charge carriers in the neutral state; therefore, charge carriers must be provided extrinsically through doping induced charge separations. In the PL spectra shown in **Figure 1.16**, the PL intensity quenches as the acceptor strength increases, and the PL quenching can be attributed to doping induced charge separation between P3HT and the dopant that suppresses the exciton PL emission. The UV-Vis-NIR of P3HT:PCBM composite thin films doped with different acceptor-T were also measured and are shown in **Figure 1.17**, where about six distinct peaks were observed. The peak at around 335 nm is attributed to the PCBM. It is believed that the peak around 515 nm corresponds to π-π* transitions in the conjugated segments of P3HT, and that this peaks' intensity is heavily influenced by the film thickness [13]. The peaks around 560 and 610 nm are believed due to inter-chain π–π stacking or polymer solid state H-type aggregates packing, where the Frenkel type inter-chain exciton bandwidth *W* can be estimated using the 560 nm and 610 nm peak intensities and is shown in **Figure 1.18** [13]. And lastly, the peaks between 600-900 nm are from polaron bands or charge transfer bands induced by doping. In recent years, several research groups have reported that increased absorption at the shoulder peaks at 560 nm and 610 nm are directly related to the increased solid-state H-type aggregates packing order [13-15].

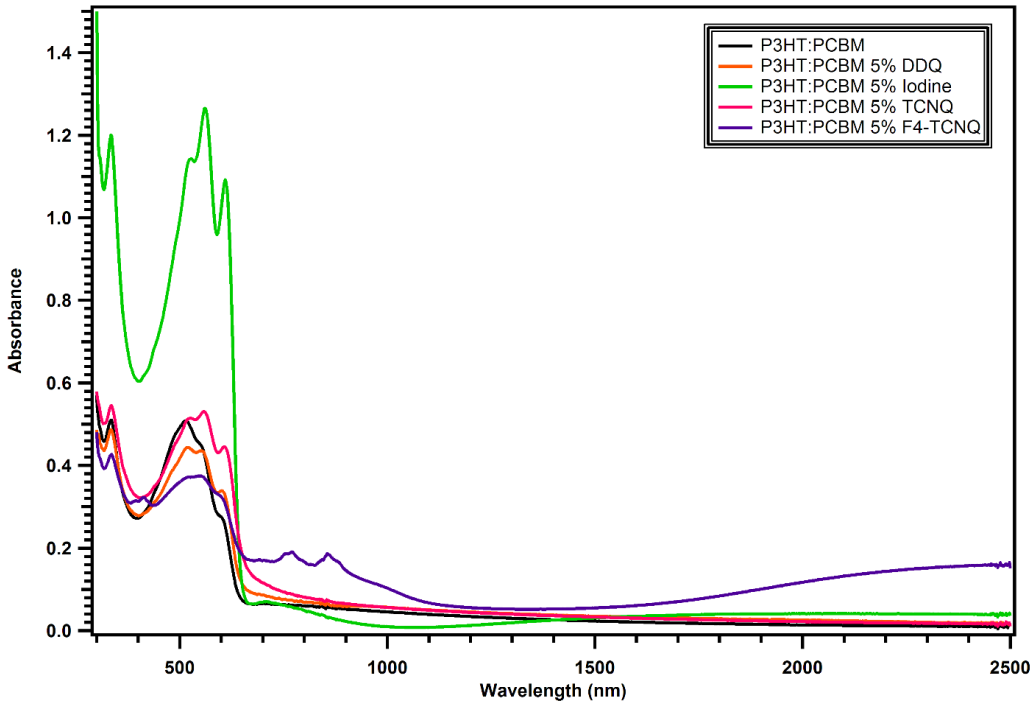

Figure 1.17 UV-Vis-NIR absorption spectra of P3HT:PCBM thin films doped with various acceptor-Ts.

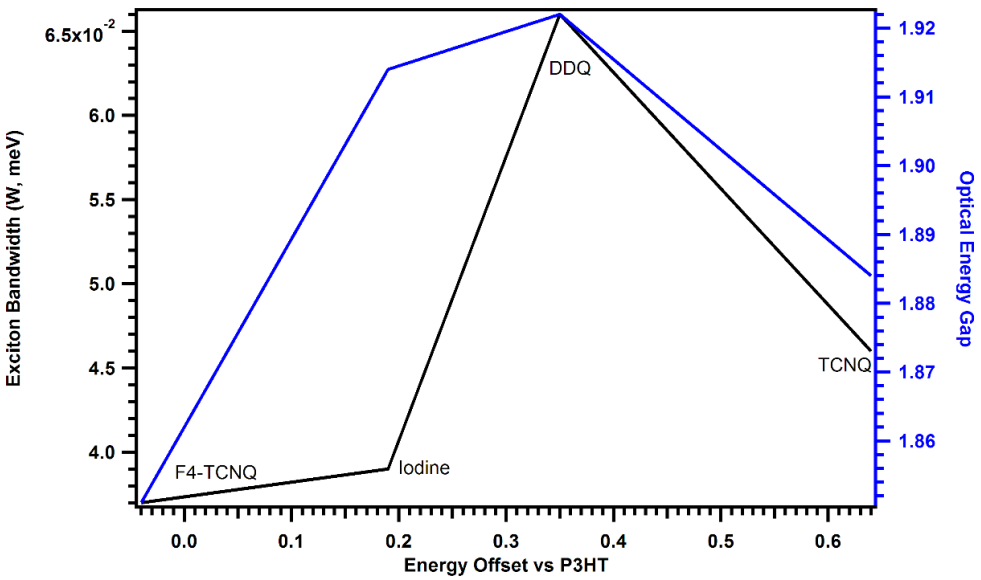

Figure 1.18 Exciton Bandwidth and optical energy gap vs. acceptor strength.

Baghgar *et al*. mentioned P3HT aggregates can adopt either J- or H-aggregate configurations which favor intra-chain and inter-chain order respectively [16]. H-aggregates exhibits blue-shift of absorption peak as compared to non-aggregates due to higher excited state energies, while J-aggregates exhibits red-shift absorption peak as compared to non-aggregates due to lower excited states energies [17]. UV/Vis and PL techniques should be run in conjunction with each other because the entire matrix may absorb but only the most ordered segments may be obvious in PL [18-19]. It is important to know that the 0–0 transition is the lowest energy absorption feature [18]. One additional parameter to characterize P3HT thin film aggregates is their exciton bandwidth *W* as estimated from the two vibronic shoulder peaks of 560 nm and 610 nm and as shown in **Figure 1.18** [20]. It is interesting to note that F4-TCNQ doped samples has the smallest exciton bandwidth of about 37 meV. It is well known that the exciton bandwidth is inversely proportional to the charge transport properties of the material meaning lower *W* leads to higher conductivities due to higher charge mobility [21].

Raman spectroscopy was also used to investigate the doping to the bonding modes in the P3HT as seen in **Figure 1.19**. The 1300-1600 cm^{-1} region is attributed to the carbon to carbon stretching modes for C-C and C=C. We observed small shifts in the C=C band in the 1440-1460 cm^{-1} range. Shifting in peak position in this range is small but indicates structural changes from benzoid to quinoid in the polymer backbone. With the addition of TCNQ, the peak position of pure P3HT and the TCNQ doped sample are nearly similar and this relationship is seen in the UV-Vis-NIR spectra as well. DDQ has a very small doping effect and hs a small shifting the C=C band again seen as a small increase in absorbance past 600 nm. Iodine and F4-TCNQ generate a greater magnitude in the shift of the Raman spectra showing these stronger acceptors have a higher doping induced morphological effects. We also observed Raman bands in the 1650-1700 cm^{-1} associated with the $F4\text{-}TCNQ^{-}$ anion as spectra are similar to the H-aggrgate type of P3HT seen by Gao *et. al.* [22].

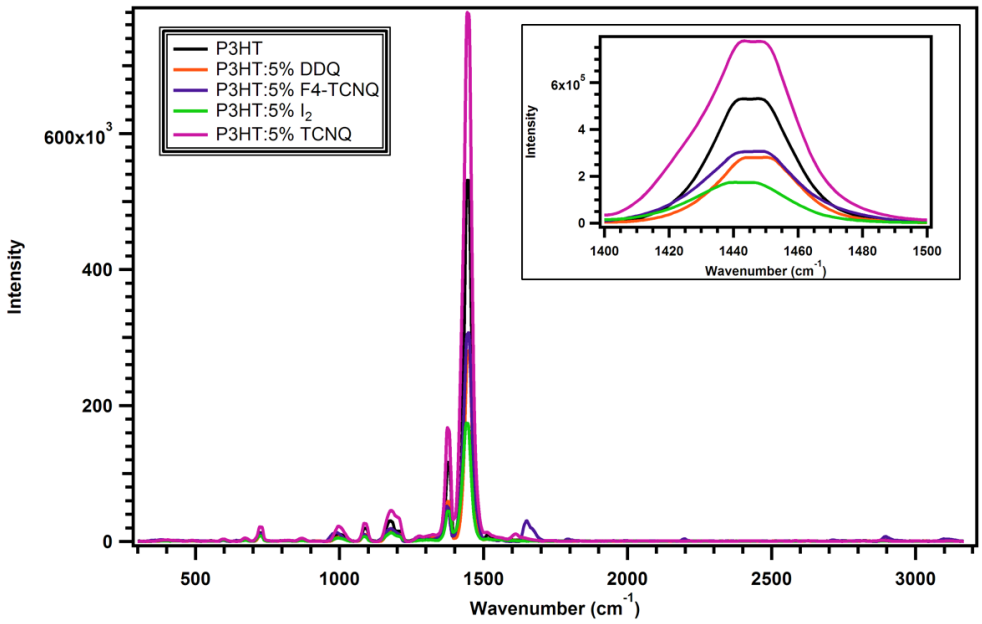

Figure 1.19 Raman spectra of P3HT doped with various acceptors.

X-ray diffraction (XRD) was also used to investigate the crystallinity and solid-state packing of different polymer samples doped with various acceptors. As shown in **Figure 1.20**, the main peak at around $2\theta = 5.255^{\circ}$ corresponds to the (100) direction plain which is the alkyl side chain direction when the P3HT is in the most popular edge-on packing style. As acceptors are introduced, the peak positions shifts slightly with a deviation of $\pm\ 0.06^{\circ}$. One of the first observations we had was that for the F4-TCNQ doped sample, the main peak completely disappears due to the complete disruption of crystallinity in that direction. For other dopants the enhancement of the main peak is observed. Enhancement of this peak is indicative of more crystallites in the film having this orientation. As shown in **Figure 1.21**, while looking at the nano-crystallite size, it seems the dopants all reduce this value. Unfortunately, for the F4-TCNQ doped sample, we noticed its XRD spectra has no peaks indicating complete disruption in crystallinity. Overall, we see that the morphology is drastically changed upon doping.

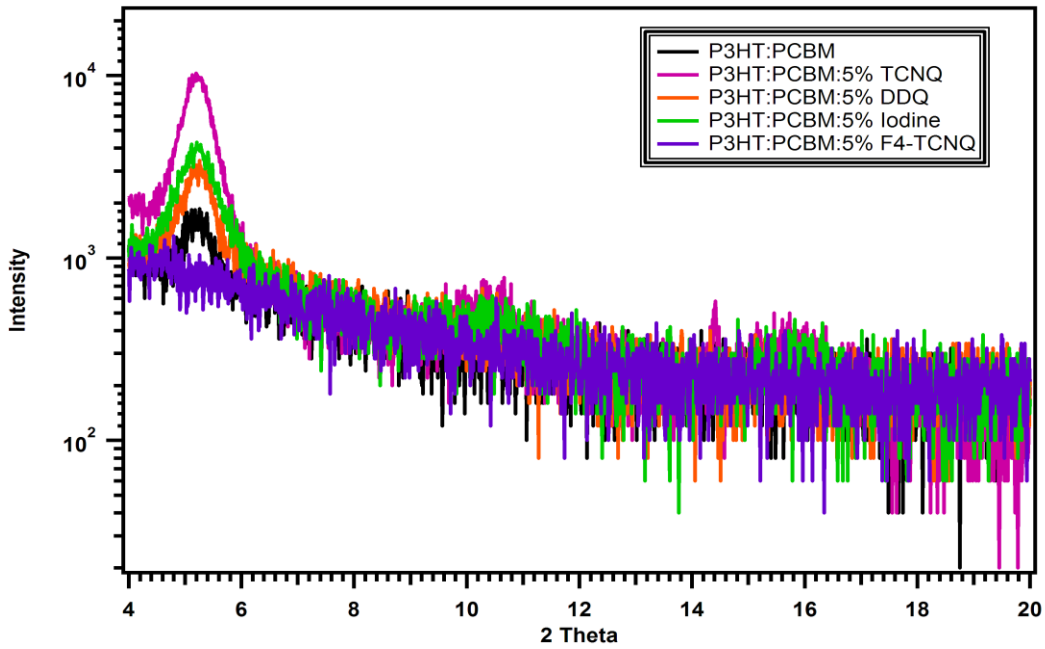

Figure 1.20 XRD spectra of P3HT thin films doped with various acceptors.

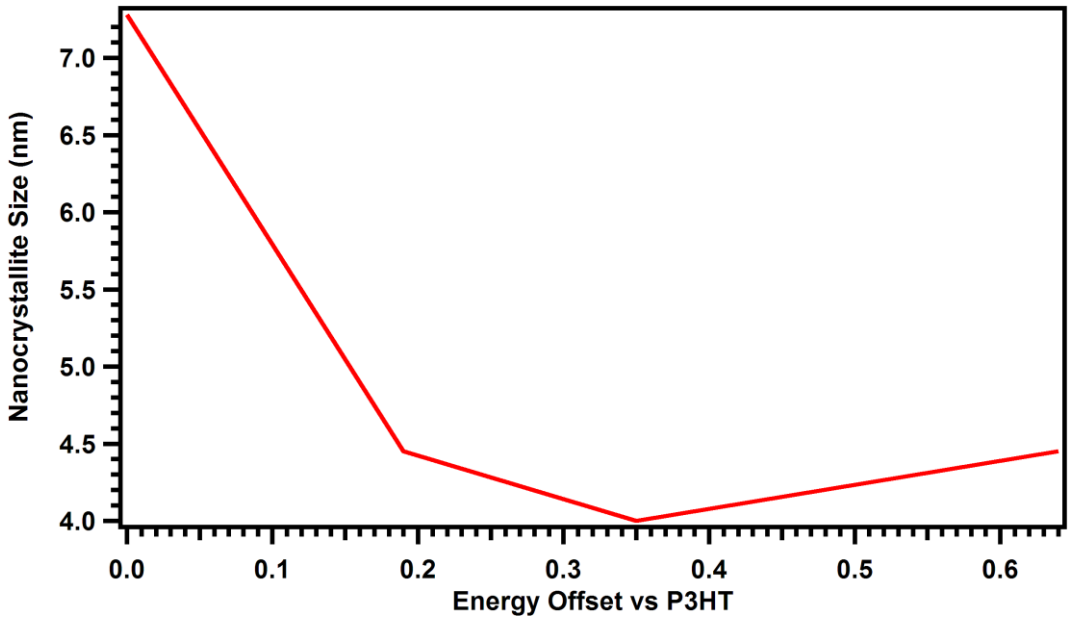

Figure 1.21 The P3HT Edge-on vertical (Z direction) inter-layer spacing (nanocrystallite sizes) versus acceptor strength (F4-TCNQ could not be calculated due to poor XRD spectra).

Atomic Force Microscopy (AFM) was also utilized to study surface morphology of the thin films (The AFM images are available upon request). Using the average surface roughness values obtained from the AFM, the surface roughness was plotted against the frontier orbital offset of the dopant relative to P3HT as shown in **Figure 1.22**. We see that the bigger molecular dopants such as TCNQ and F4-TCNQ, have drastic effects on the surface roughness of the thin films. Also, F4-TCNQ doping induces the roughest surface

due to the summation of strong doping and large molecular size. The AFM images along with XRD indicate that some conformational changes in P3HT occur upon doping. It is possible that the P3HT chains self-organize into a more ordered structure which can lead to changes in charge carrier transport capability and the TE performance of the films [23].

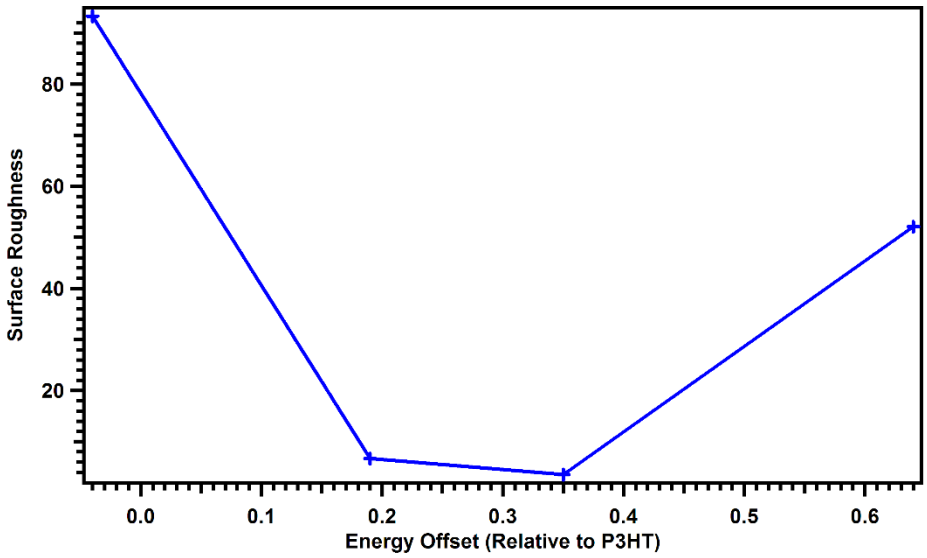

Figure 1.22 Average RMS surface roughness of P3HT:PCBM thin films doped with various acceptors.

Lastly, the thermoelectric properties of these films were studied in the dark and under illumination to observe how the different dopants effects these properties. **Figure 1.23** displays the Seebeck coefficients and the electrical conductivity of P3HT:PCBM samples doped with various acceptors. As expected, the stronger acceptor yield the highest electrical conductivity while also leading to the lowest Seebeck coefficient. This trend is typically seen in literature and is a result of the inverse relationship between the Seebeck coefficient and carrier concentration (as illustrated in equation 1.3). The Power Factor and *ZT* values (shown in **Figure 1.24**) were estimated using the Seebeck values, measured electrical conductivity, literature cited thermal conductivity of 0.1 W/m*K for P3HT:PCBM, and the absolute temperature of 300 K. The thermal conductivity value used was experimentally measured by Duda *et.al* for 1:1 P3HT:PCBM thin films [24]. Note that they were able to determine that the relationship between crystallinity and thermal conductivity. To our knowledge, no one has studied the thermal conductivity versus doping type or concentration, we assumed all films have the same or similar thermal conductivity. The F4-TCNQ doped films exhibited the highest PF and ZT values under study conditions.

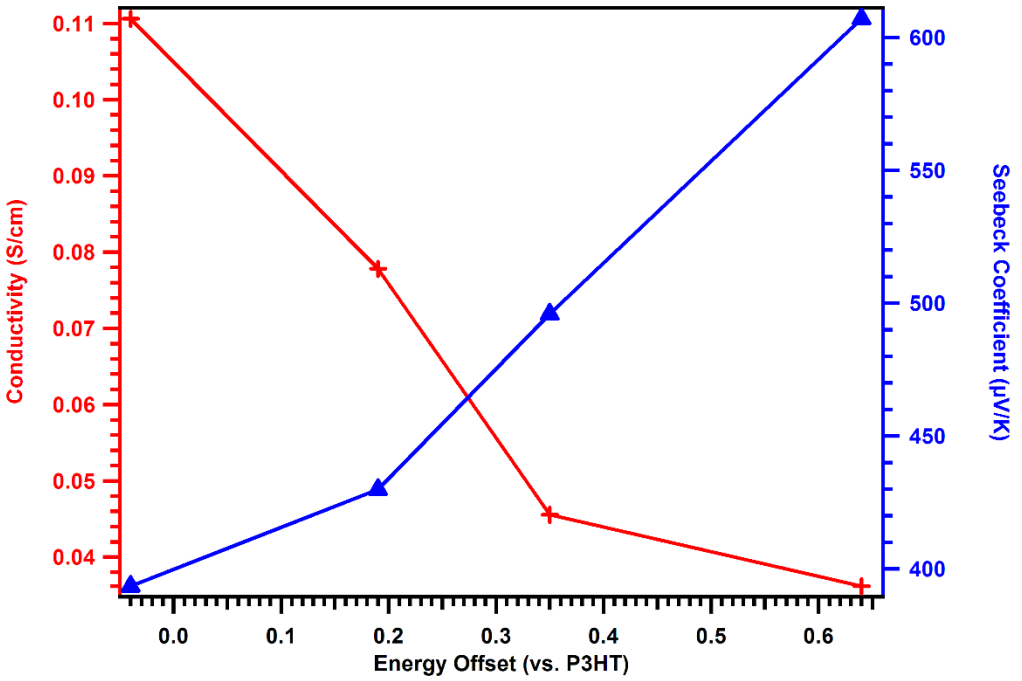

Figure 1.23 The conductivities and Seebeck coefficients of P3HT:PCBM composites versus the frontier orbital energy offsets of the dopants relative to P3HT.

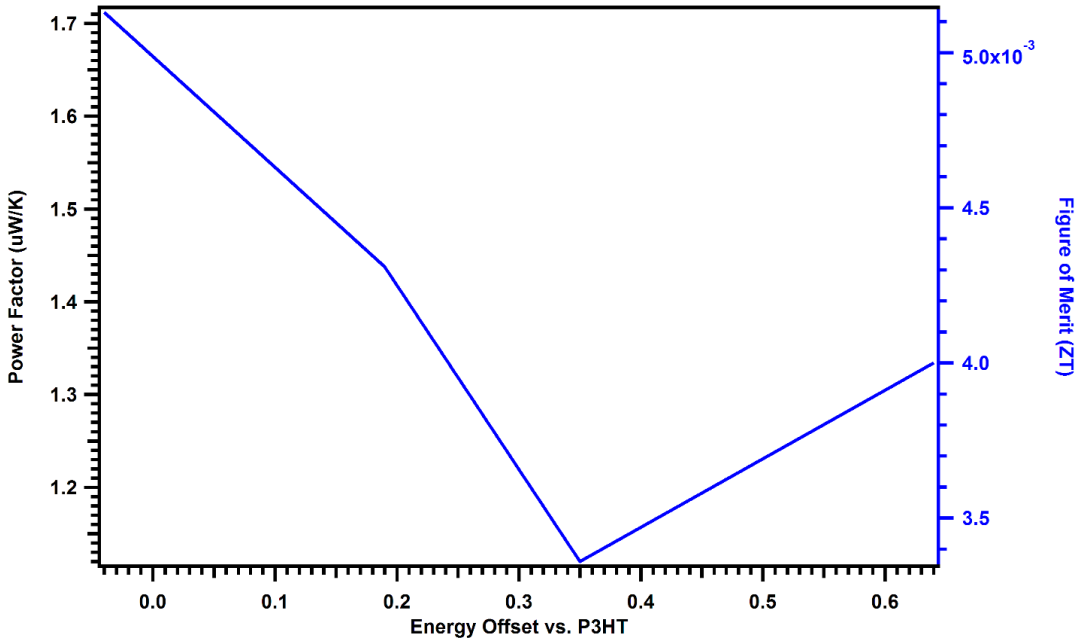

Figure 1.24 The thermoelectric Power Factor and the Figure of Merit (ZT) of Dopant:P3HT:PCBM composites versus the energy offset of the dopant relative to P3HT.

1.5 Summaries and Conclusions

In summary, the PE/TE and TE/FET dual conversion and dual modulation materials and devices have been successfully demonstrated. The correlations of the frontier orbital levels and offsets versus electrical and thermoelectric properties of a series of PCBM:P3HT:dopant ternary composites were also systematically evaluated. The UV-Vis-NIR spectroscopy, photoluminescence quenching, and solution dynamic light scattering studies reveal that strong electron accepting strength of the dopant acceptors can result in P3HT main chain aggregations even in solution. In the solid-state thin films, UV/Vis spectroscopy, atomic force microscopy (AFM), and X-ray diffraction (XRD) reveal that presence of acceptors increases surface roughness and disrupt the crystallinity of P3HT or P3HT:PCBM thin films. As the orbital offsets (or energy barriers) between HOMO of P3HT and LUMO of dopants increases from F4-TCNQ to iodine to DDQ and finally to TCNQ, the electrical conductivity decreases (possibly due to energy barrier increases), the Seebeck coefficients increases (due to charge carrier density decreases), while the thermoelectric power factor and the thermoelectric figure of merit ZT initially decreases from F4-TCNQ to DDQ (possibly due to dominant electrical conductivity contribution decrease) and then increases slightly to TCNQ (possibly due to dominant Seebeck contribution increase). This work could be helpful to understand the mechanisms of chemical doping of conjugated polymers at the molecular level and their correlations to bulk thermoelectric properties for a variety applications.

1.6 Next or Future Researches

While the P3HT:PCBM:Iodine PE/TE and TE/FET dual conversions and dual modulations have been preliminarily and successfully demonstrated, there are numerous parameters need to be systematically surveyed and optimized, and some fundamental scientific principles and mechanisms still need to be further investigated or clarified. For instance, chemical structures and types of potential optimal photoelectric and thermoelectric dopants, the magnitude or optimal frontier orbitals of both thermoelectric and photoelectric dopants in relation to P3HT or another candidate polymers, heating temperatures, radiation light being used, film morphologies, processing protocols, and particularly the interactions (both positive or negative) of each conversion and resulting charge transport to each other. The thermoelectric power factor and/or thermoelectric figure of merit (*ZT*) values (instead of the Seebeck coefficients) also need to be systematically evaluated. Potential applications of such multi-functional materials also need to be systematically evaluated.

2. Progresses on Development of a New DB-ffA Block Copolymer and Structure/Morphology/Property Correlation Studies of the DBfA Type Block Copolymers

2.1 Proposed Research

In order to further understand or address the fundamental scientific questions of how the inter-molecular orbital coupling and the molecular solid state thin film morphology could affect the photo generated exciton dissociation and charge carrier transport, a **DBfA** type block copolymer system has been previously developed by our group [25], where the photoelectric power conversion of the **DBfA** based solar cell is found to be about two orders of magnitude larger than the corresponding **D/fA** simple blend. Our explanation for such improvement of the block copolymer versus simple blend is due to 1) Photo generated exciton dissociation is more efficient due to both **D** and f**A** domain size are being controlled within typical Frenkel exciton diffusion range of less than 20 nm; and 2) Photo generated charge carriers (both electrons and holes) now have more bicontinuous transport pathways toward their respective electrodes. Also, the fluorine side groups further improved the **D** and **A** nano domain phase separation due to chemical differences between CH and CF groups. For this reason, in the proposed research, a **DB-ffA** block copolymer with increased fluorine contents in acceptor block **ffA** is proposed. Original synthetic scheme of **ffA** block for **DB-ffA** is shown in **Figure 2.1**, where the acceptor block **ffA** now contains two fluorine group of C_8F_{17} on both sides (instead of one side) of the **DB-ffA** conjugated main chain. Such polymer main chain chemical structure is expected to further enhance the D and ffA block nano domain phase separations and is expected to result in even higher photoelectric conversion efficiencies. Additionally, correlation studies of **DBfA** type block copolymer optoelectronic properties versus its chemical structures and solid state morphologies shall be systematically investigated.

2.2 Development of DB-ffA

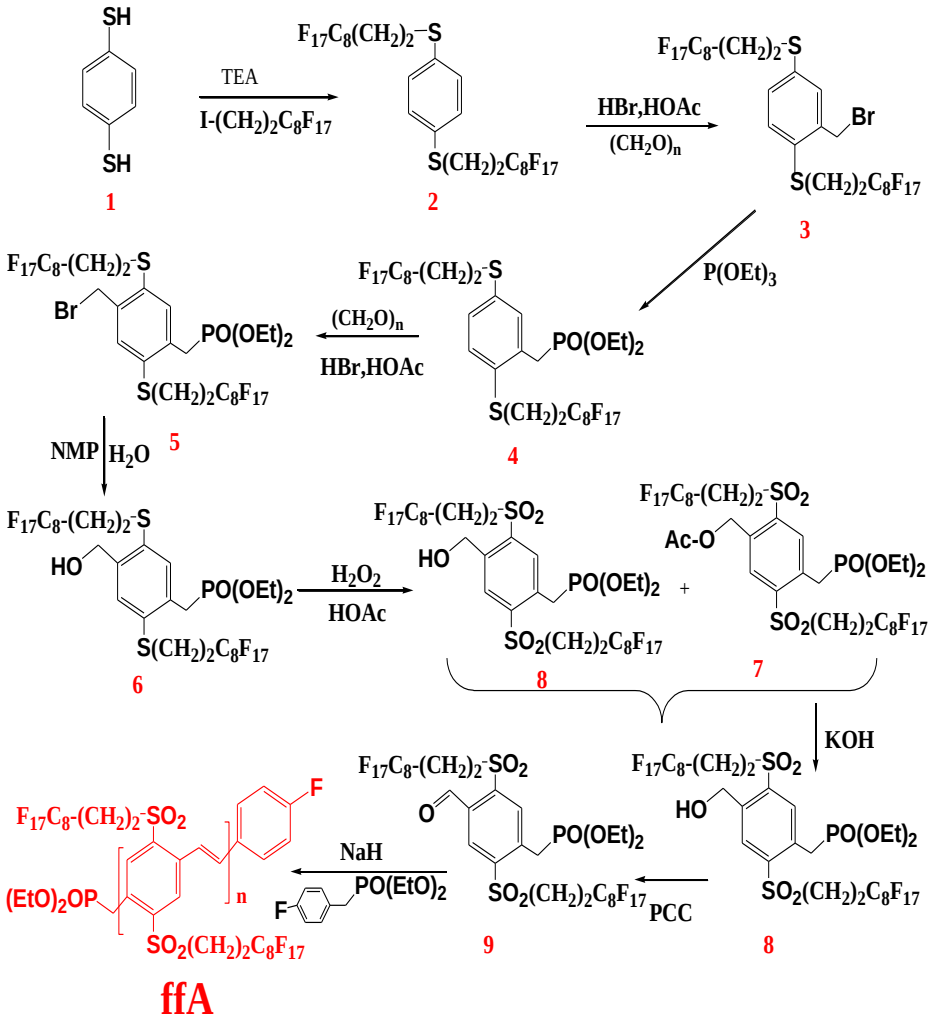

Figure 2.1 Synthetic scheme of the proposed **ffA** monomer and block copolymers.

During project period, compound **6** in **Figure 2.1** was successfully synthesized and characterized via five steps. However, after sulfides were oxidized into sulfone, due to solubility difficulties of **7** and **8**, the synthetic scheme in **Figure 2.1** was modified to **Figure 2.2**, where instead of oxidizing compound **6** to form sulfone compounds of **7** or **8**, the hydroxy-methyl CH_2OH group was oxidized directly into aldehyde group resulting in a formation of compound **7b** (successfully synthesized and characterized) as shown in **Figure 2.2**. **Figure 2.3** exhibits MALDI-TOP spectrum of **ffA** block, and **Table 2.1** lists all calculated fragmentations of **ffA-b** polymer block. Based on the MALDI spectrum and the calculations, it appears at least four (4) repeat unit **ffA-b** block was identified. Unfortunately **ffA-b** polymer block was still not very soluble, and soluble derivatives of **ffA** would need new side chain monomer synthesis from first step which is very time

consuming, so the **ffA** block effort was temporarily on hold pending additional literature research and evaluations.

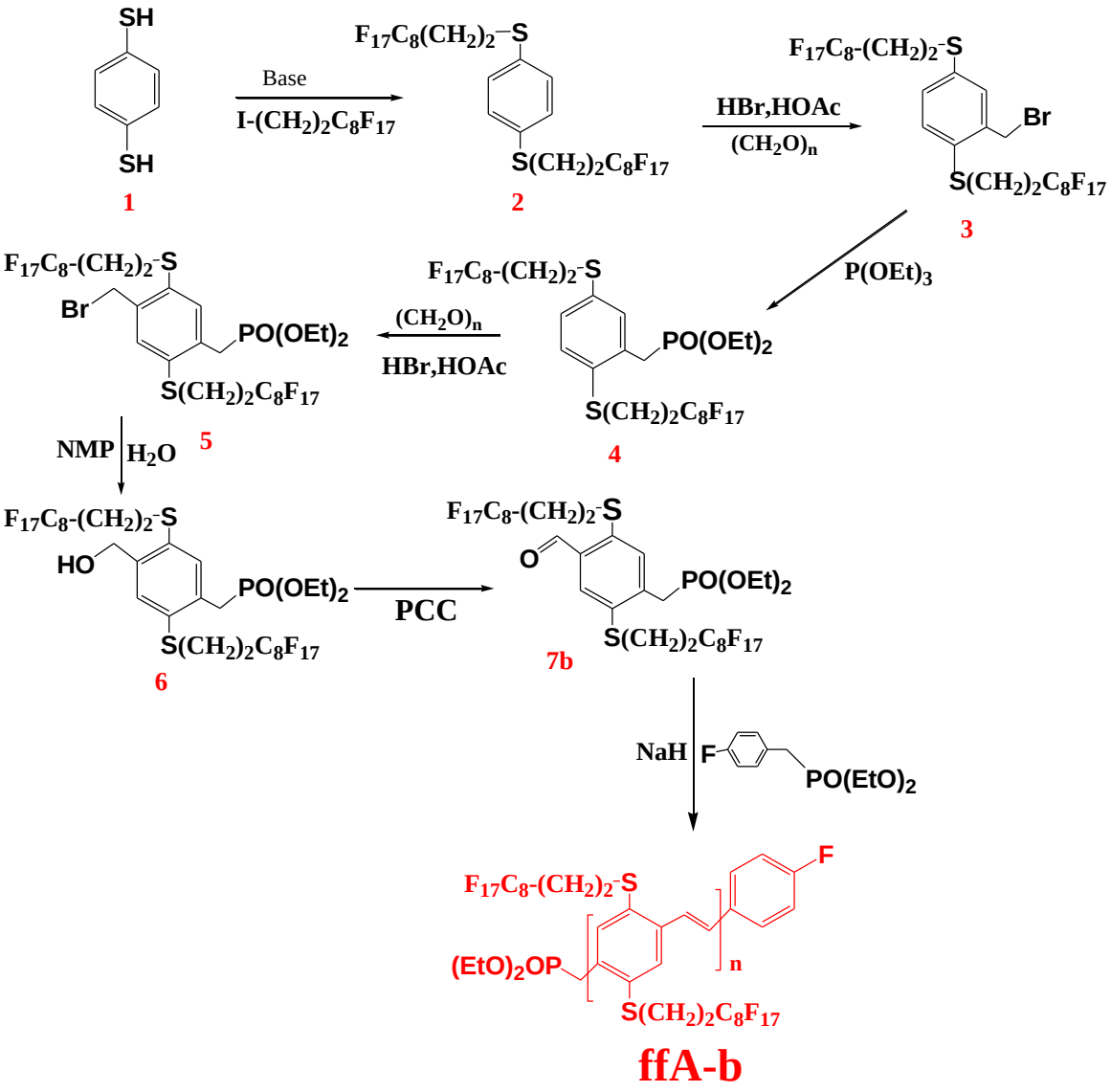

Figure 2.2 Revised synthetic scheme of a new di-sulfide and di-fluorinated ffA-b polymer block.

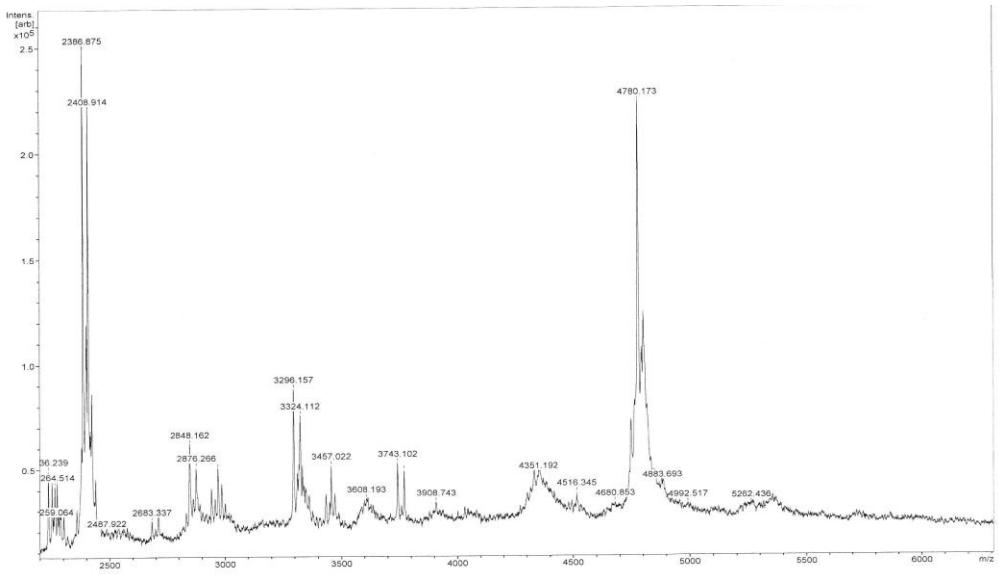

Figure 2.3 MALDI-TOP spectrum of ffA-b polymer block.

Table 2.1 Calculated fragmentations of ffA-b polymer blocks

Repeat Unit	FW	FW- 1 side chain	FW- 2 side chain	FW-phosphonate side	FW-terminator side	FW-both (T & P)
1	1310	831	352	1159	1213	1062
2	2614	2135	1656	2463	2517	2366
3	3918	3439	2960	3767	3821	3670
4	5222	**4743**	4264	5071	5125	4974
5	6526	6047	5568	6375	6429	6278

2.3 Correlations of Chemical Structure/Bridge Effects to the Optoelectronic (OE) Properties of DBfA Type Block Copolymers

A series of **DBfA** type block copolymers with a bridge unit (B) containing one methylene unit (C1), two methylene units (C2), four methylene unit (C4) and six methylene unit (C6), as well as a **DfA** block copolymer without bridge unit were successfully developed in our lab [25]. A systematic study to correlate **DBfA** bridge units or their morphologies and optoelectronic properties were pursued [26]. Specifically, photoluminescence spectra of D, D/fA blend, DfA and DBpfA in THF solution are shown in **Figure 2.4**, where the concentration of D repeat unit are kept at $1x10^{-}5M$ in all sample solutions, and only D is being excited at 530nm and fA is not excited. The data shows that PL of **D/fA** blend, **DfA**, and **DBpfA** quenched up to about 26% as compared to pristine D, with **DB1fA** consistently quenched strongest than other **DBpfAs**. Similarly, as shown in **Figure 2.5**, when the acceptor fA block is excited at 370nm, and **fA** repeat unit concentration is fixed at $1x10^{-}5M$, the PL of **D/fA** blend, **DfA**, and **DBpfAs** are quenched up to 88% as compared to pristine **fA**, again with **DB1fA** quenched strongest than other DBpfAs.

Stern-Volmer (SV) PL quenching experiment and the SV-Plot is a standard method of determining a PL quenching coefficient between two molecular species in solution. When the **fA** block repeat units concentration is fixed at $2.8x10^{-5}M$, as the concentration D increases, the PL of **fA** is quenched gradually as shown in **Figure 2.6**. After subtracting the energy transfer (ET) contributions [9], the charge transfer induced SV-Plot is shown in **Figure 2.7**, where a PL quenching coefficient of K_{sv}= 19222 is obtained for the **fA/D** pair.

In the donor PL quenching case, the PL quenching of D in **D/fA** blend is attributed mainly to the photo induced electron transfer from D block to fA block via collision in THF, while the PL quenching of D in **DfA** and **DBpfAs** could be attributed to the photo induced electron transfer from D block to **fA** block via collision as well as intra-molecularly via the bridge B unit. In the **fA** PL quenching case, the PL quenching of **fA** in **D/fA** blend is attributed mainly to the photo induced electron transfer from D block to **fA** block via collision in THF, while the PL quenching of fA in **DfA** and **DBpfAs** could be attributed to the photo induced electron transfer from D block to fA block via collision as well as intra-molecularly via the bridge B unit. One interesting observation is that the PL quenching is not the strongest for the conjugated block copolymer without bridge (**DfA**), and this can be explained by at least four stable states of different twist angles (with lowest energy state at a seventeen (17) degree twist angle) between the **D** and **fA** conjugated plains as predicted from the First Principle 3-21G calculation method (**Figure 2.8/Table 2.2**) [30].

Figure 2.9 and **Table 2.3** exhibits photo JV curves and data of the solar cells fabricated from **DBfA(C0-C6):PCBM** composites, where the best performance cell was from **DBfA** with C1 bridge unit. From these results, it appears the best OE property (largest V_{oc} and I_{sc}) corresponds to the **DBfA(C1) or DB1fA** [26].

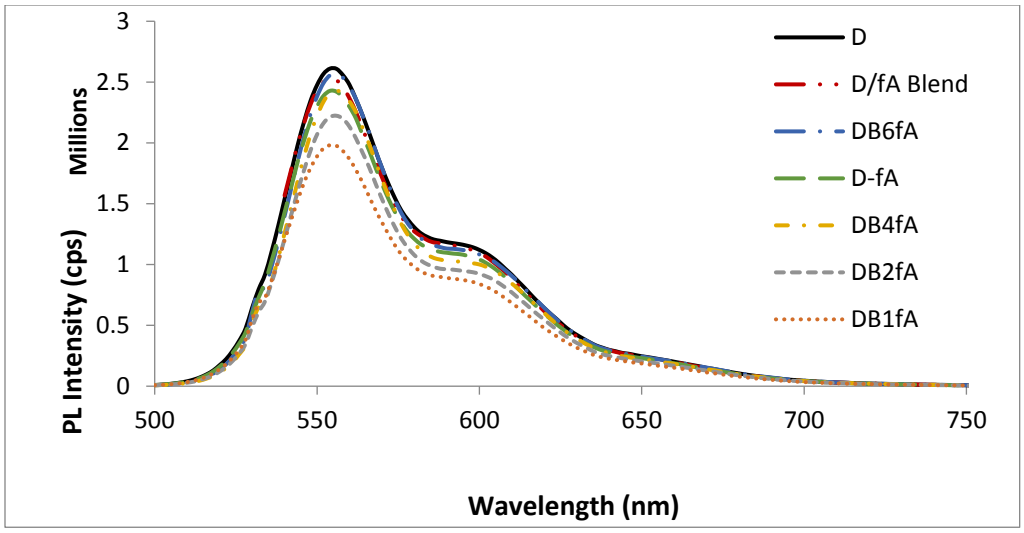

Figure 2.4 PL Spectra of D, D/fA, DfA, and DBpfAs, where D repeat unit concentrations are $1x10^{-5}$M in all solutions (Ex: 530nm).

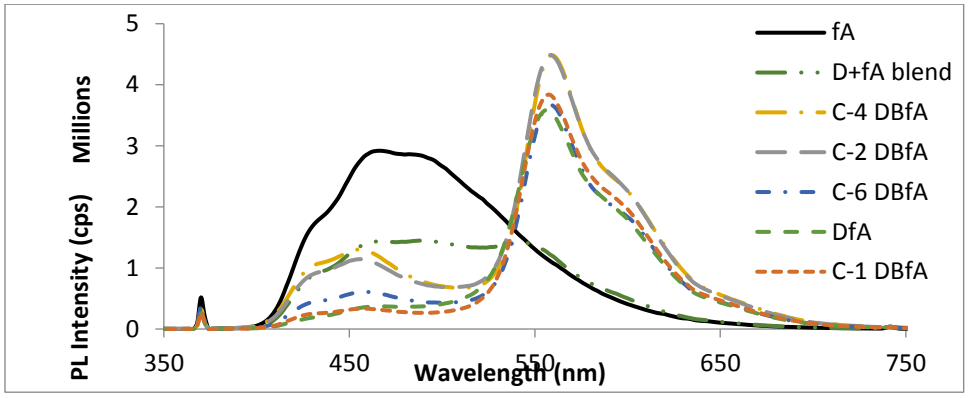

Figure 2.5 PL Spectra of fA, D/fA, DfA, and DBpfAs, where fA repeat unit concentration $1x10^{-5}$ M in all solutions (Ex: 370nm)

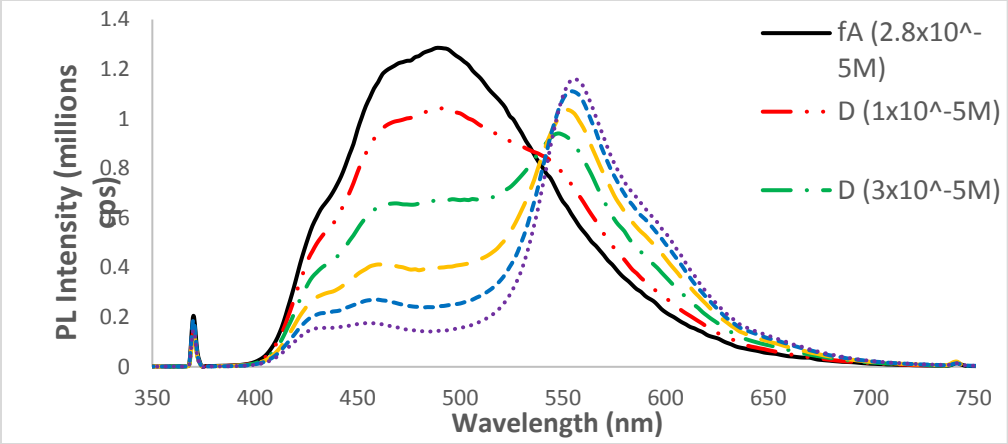

Figure 2.6 Stern-Volmer PL spectra of fA quenched by different concentrations of D, where fA repeat unit concentration $2.8x10^{-5}$ M and excitation at 370nm.

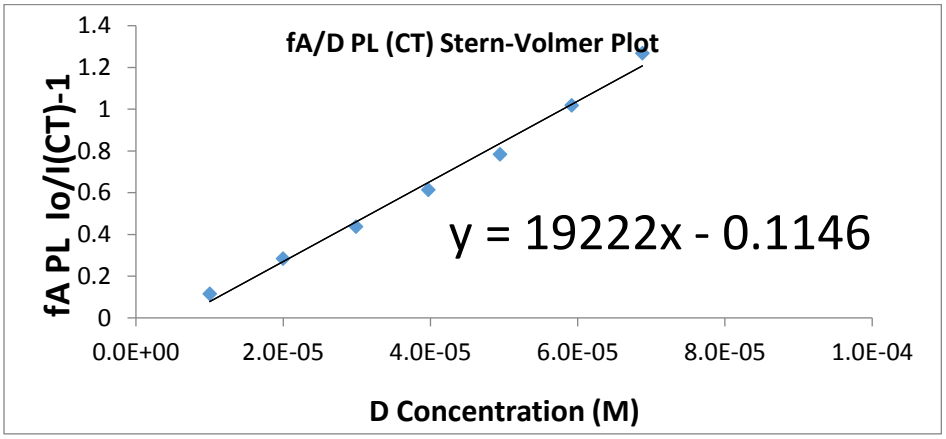

Figure 2.7 Stern-Volmer plot of fA quenched by different concentrations of D based on PL spectra shown above, where I (CT) represents PL intensity dropped due to charge transfer (CT).

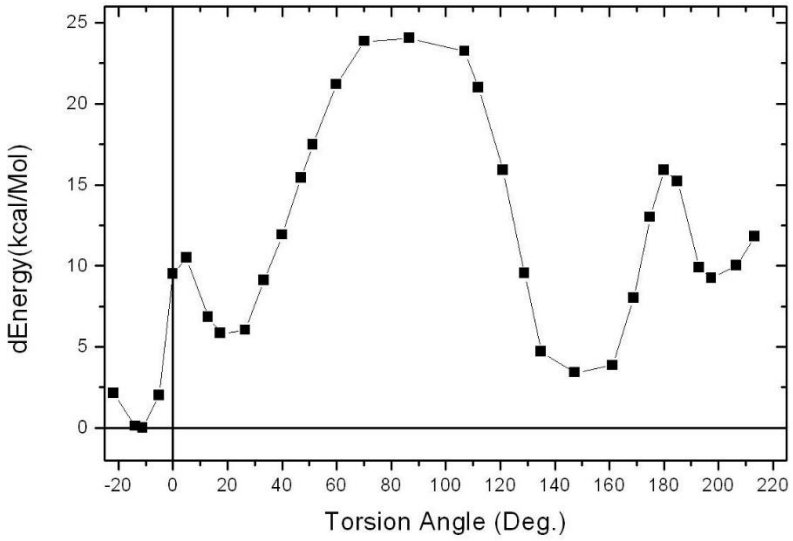

Figure 2.8 Torsional potential curve calculated for the **DfA** at different twist or torsion angles of **D** from the **fA** blocks. Zero angle corresponds to where the Pz or pi electrons of all benzene rings of the **D** and **fA** blocks and the bridge double bond are in the same conjugation plane. Positive angle corresponds to clockwise rotation of **D** viewed from **fA** [30].

Table 2.2 Optimized twisting angles of **D** from **fA** in **DfA** corresponds to the modeled minimum potentials as shown in **Figure 2.8**.

Minimum #	**D/fA** Rotation Angle (Deg.)
1	-17
2	21
3	149
4	198

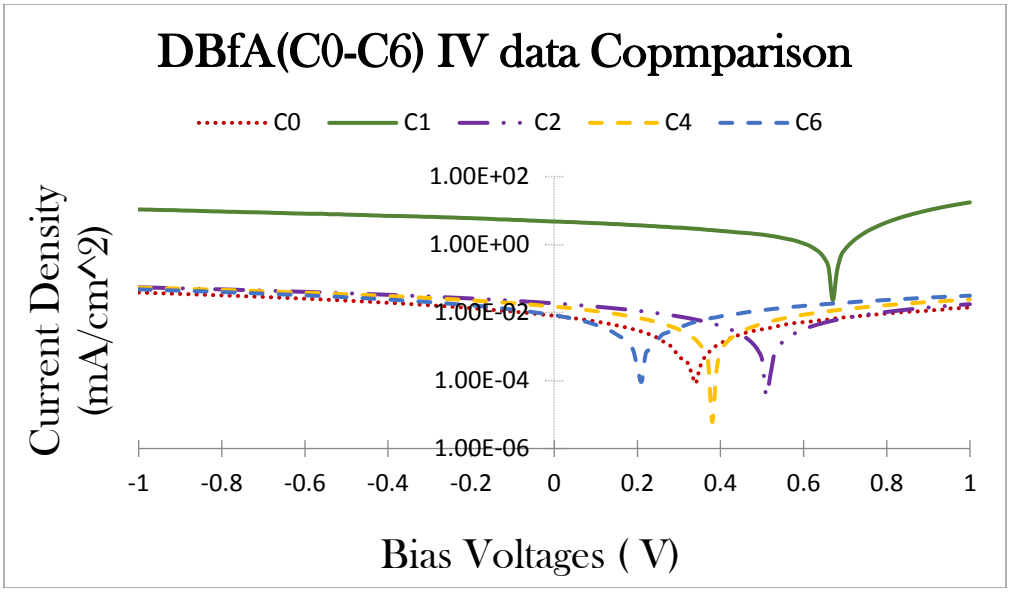

Figure 2.9 DBpfA (p=0, 1, 2, 4, 6) photo JV data comparisons.

Table 2.3 Solar Cell Performance of DBfA(C#)

Polymer's	**Voc**	**Jsc**	**FF%**	**PCE%**
DfA (C0)	0.34	0.01	19.85	0.001
DBfA (C1)	0.67	5.89	31.72	1.56
DBfA (C2)	0.51	0.02	25	0.003
DBfA (C4)	0.38	0.02	25	0.002
DBfA (C6)	0.21	0.01	25	0.0007

2.4 Correlations of Morphology to Optoelectronic (OE) Properties of DBfA(C1) Block Copolymer

In order to correlate morphologies to optoelectronic properties, **DBfA(C1)** (or **DB$_1$fA)** was selected as the initial test sample. Specifically, thin films of **DBfA(C1)** was thermally annealed at three different temperatures of 100, 150 and 200^{o}C and their morphologies and optoelectronic properties were compared and evaluated. All polymer thin film samples are prepared by spin coating polymer solutions (typically 15.0 mg polymer dissolved in 1.0 ml o-dichlorobenzene) to a thickness of 1-2 micron on regular ITO substrates. For 100,150, & 200^{o}C thermally annealed and dried films, the 2D phase and amplitude images of atomic force microscopy (AFM) at half micron scales of films are shown in **Figures** 2.**10**. As the AFM images reveals, at 150^{o}C, **DBfA(C1)** film somehow exhibits finest phase separation or most fine/smallest average domain sizes, while the 200^{o}C film exhibited largest domain sizes. It is known that the film morphology and domain sizes plays a vital role for optoelectronic properties due to exciton dissociation requires large **D/A** interfaces or small D/A domain sizes, while the charge transport requires continuous morphology or large domain sizes.

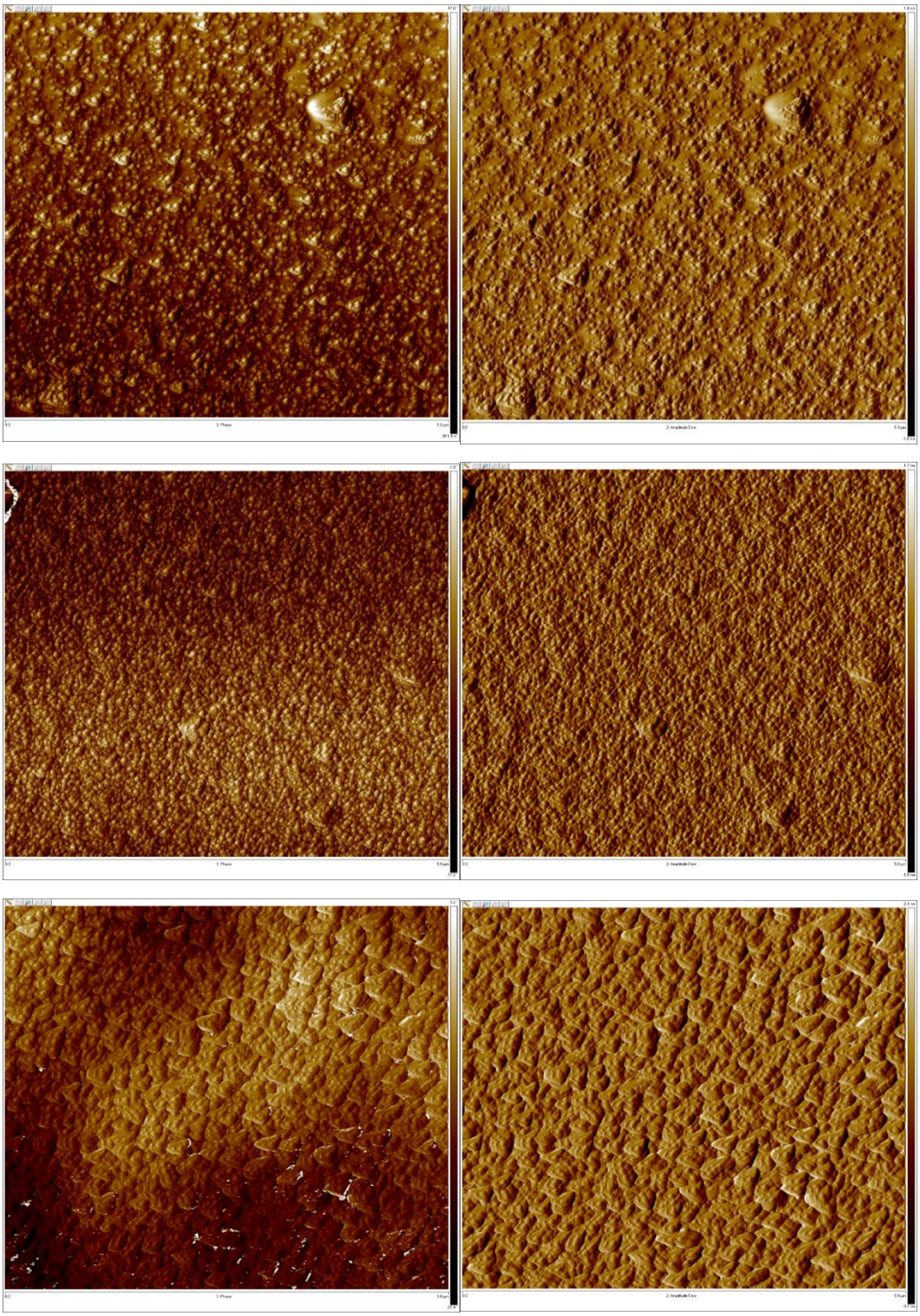

Figure 2.10 AFM images of **DBfA**(C1) annealed at 100, 150 & 200^{o} C respectively top to bottom (left) Phase 2D and (right) Amplitude 2D.

Figure 2.11 exhibit light photo JV curves of the solar cells thermally annealed at three different temperatures. In this case, 100°C film exhibits the best optoelectronic solar cell performance among all three temperatures films. Our explanation for the optimal performance at 100°C is that too small domain sizes at 150°C may limit the continuous charge transports due to too much interruptions in charge transport pathways, and that too large domain sizes at 200°C can result in smaller D/A interface and therefore reduced exciton dissociations. Therefore an optimum or middle roughness or grain size of the film exhibit the best optoelectronic performance.

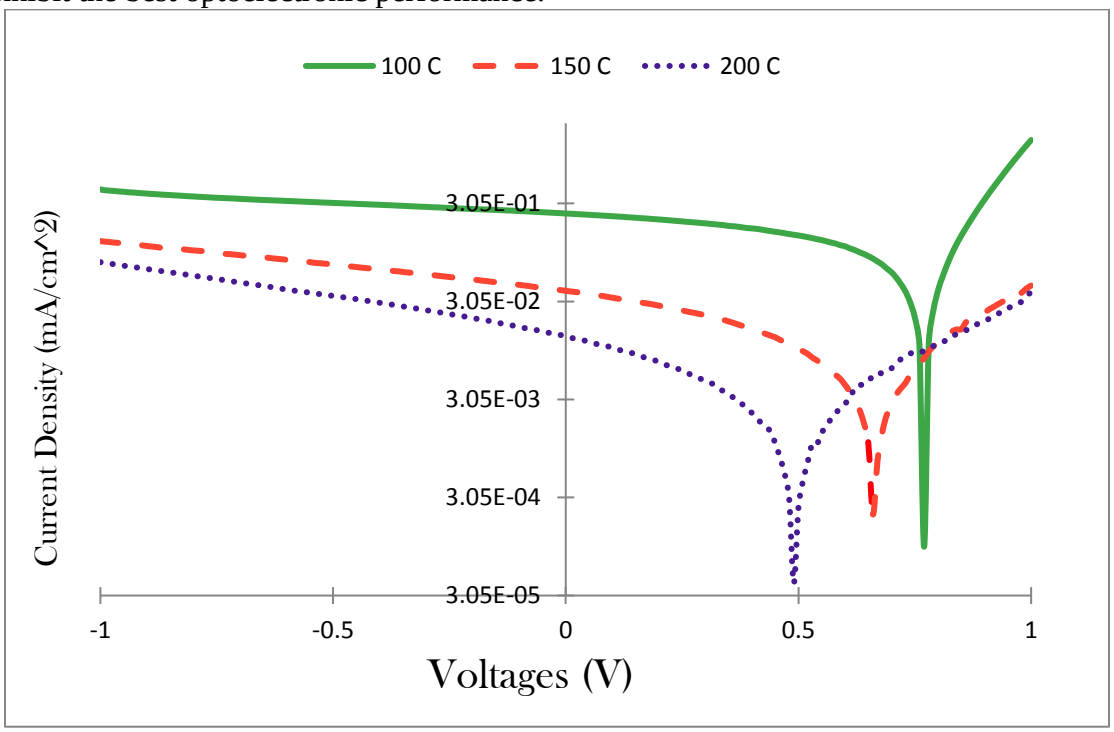

Figure 2.11. Light JV curves of **DBfA(C1)** solar cells annealed at 100°C, 150°C and 200°C respectively.

2.5 Summaries and Conclusions

In summary, a new benzene disulfide and di-fluorinated monomer **7b** and new disulfide and di-fluorinated functionalized conjugated polymer block **ffA-b** were successfully synthesized and characterized, but once the sulfides were oxidized into the desired sulfone acceptor form, the **ffA-b** become insoluble. Soluble analogues may be developed but that would involve synthetic adjustments from first synthetic step. The correlation studies between chemical structures, morphology, and electronic/optoelectronic properties of the **DBfA** systems is being evaluated systematically. Important observations/conclusions include that 1) that **DB$_1$fA** block copolymer containing one methylene unit exhibited the strongest PL quenching and the best optoelectronic property (The PL quenching of no-bridge **DfA** or more bridged **DB$_p$fA** were much less); and 2) an intermediate thin film gran size appear to exhibit best optoelectronic performance in a **DB$_1$fA** block copolymer.

2.6 Next or Future Research

The next or future research efforts shall be continued systematic studies of block copolymer chemical structures versus solid state morphologies versus device properties at molecular scales. In particular, the mechanisms or reasons of an optimal bridge length (C1 bridge) and an optimal thermal annealing temperature (100^{o}C) and its morphology need to be further investigated or clarified.

3. Progresses on Investigations of a Series New Octabutoxy-Metal-Pthalocyannine Complexes (OB-MPc) for Optoelectronics

3.1 Proposed Research

In order to answer the question of correlations between frontier orbital offset δE_1 versus the materials photoelectric effect as shown in **Figure 1.1**, a composite donor/acceptor pair containing a donor type polymer (*e.g.*, Poly(3-hexylthiophene-2,5-diyl or **P3HT**) and a series of soluble octabutoxy-metal-Phthalocyanine complexes OB-MPc (products shown in **Figure 3.2**) shall be paired and evaluated for photo induced charge transfer studies. For instance, based on Marcus electron transfer model as shown in **Figure 3.1**, it is expected the photo induced electron transfer rates between P3HT and a MPc complex could be fastest when the key driving force δE_1 and the sum of key counter-driving forces (including the exciton Columbic binding energy and the electron transfer re-organization energy) are balanced. In the proposed example OB-MPc complexes where a general synthetic scheme is shown in **Figure 3.2**, the metal can be a series such as Zn, Mg, Fe, Ni, Co, Mn, *etc*. Such a molecular series appear ideal for such correlation studies due to each metal will only change frontier orbital levels but not the re-organization energies.

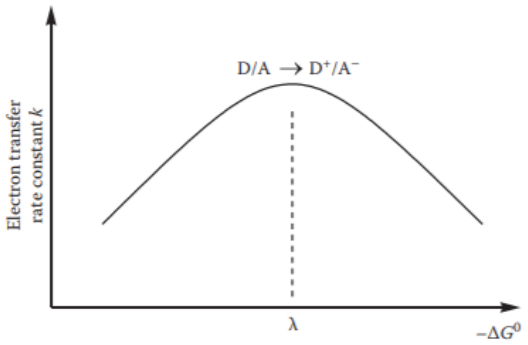

Figure 3.1 Marcus electron transfer model.

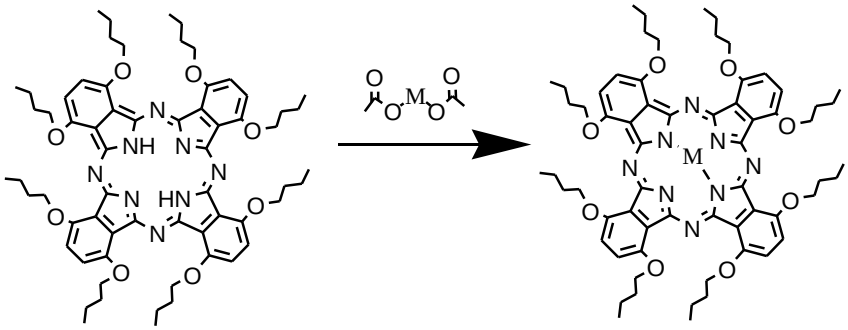

Figure 3.2 Synthetic scheme of a series of Octabutoxy-Metal-Pthalocyannine (OB-MPc) complexes to be studied for correlation of frontier orbitals offsets of P3HT/OB-MPc versus photoelectric conversions.

3.2. Synthesis, Characterizations, and Optoelectronic Studies of Octabutoxy-Metal-Phthalocyanine (OB-MPc)

Synthesis and Characterizations of M-Octabutoxy-Phthalocyanines

During the project period, a series of new side chain derivatized and soluble Octabutoxy-Metal-Phthalocyanine (OB-MPc) have been successfully synthesized and characterized [34]. Confirmation of synthesis of Metal Octabutoxy-Phthalocyanines was conducted via Nuclear Magnetic Resonance Spectroscopy (NMR) from a Bruker Advance 300 MHz spectrometer with TMS as the internal reference. All NMR samples were dissolved in deuterated chloroform ($CDCl_3$). The NMR spectra data presents the chemical shift of the internal protons of the Metal Octabutoxy-Phthalocyanines. Based on previous studies, the location of the peaks can be confirmed in conjunction with other publications.

A newly purchased Matrix-Assisted Laser Desorption/Ionization with Time of Flight Mass Spectrometry (MALDI-TOF) was utilized to determine the masses of each molecular complex. **Table 3.1** exhibits calculated/theoretical and measured molecular weights (MW) of the synthesized OB-MPc as well as several commercially available ones [34]. The molecular masses for each complex were calculated, measured, and compared with percent errors. Small discrepancies were seen for Cadmium Octabutoxy-Phthalocyanine in that observed molecular mass peaks were roughly 9 $^{g}/_{mol}$ less and 11 $^{g}/_{mol}$ more than the expected mass of around 1,201 $^{g}/_{mol}$. Ionization processes involving matrices in MALDI-TOF could be the culprit in such discrepencies. An aprotic matrix such as trans-2-[3-(4-tert-Butylphenyl)-2-methyl-2-propenylidene]malononitrile (DCTB) is a very effective matrix for several organometallic, coordination, and highly conjugated compounds with OE+ (radical) ions. It is very likely that this aromatic complex underwent one-electron reduction. Examples of this are with toluene and potassium as well as naphthalene and sodium. This protonation could, in fact, display the discrepancy seen. It is also possible that the loss of hydrogens in CH_3 attached to the ligands could explain the displayed molecular masses. For the molecular mass analysis, the matrices used were α-Cyano-4-hydroxycinnamic acid (α-CHCA), 2,5-Dihydroxybenzoic acid (DHB), and Salicylic Acid (SA).

Table 3.1 MALDI-TOF calculated and measured molecular masses of each metal complex [34].

Metal Octabutoxy-Phthalocyanine	*Calculated mass (g/mol)*	*Measured mass (g/mol)*	Δ	*Percent Error (%)*
Non-Metal Octabutoxy-Phthalocyanine	**1,091.38**	**1,091.92**	**0.50**	**0.049**
Zinc Octabutoxy-Phthalocyanine	**1,154.77**	**1,154.96**	**0.19**	**0.017**
Copper Octabutoxy-Phthalocyanine	**1,152.94**	**1,152.10**	**0.84**	**0.073**
Nickel Octabutoxy-Phthalocyanine	**1,148.09**	**1,148.82**	**0.73**	**0.064**
Cobalt Octabutoxy-Phthalocyanine	**1,148.33**	**1,148.33**	**0**	**0**
Palladium Octabutoxy-Phthalocyanine	**1,195.81**	**1,195.12**	**0.69**	**0.058**
Manganese Octabutoxy-Phthalocyanine	**1,144.30**	**1,143.79**	**0.51**	**0.045**
Cadmium Octabutoxy-Phthalocyanine	**1,201.79**	**1,1192.45**	**9.34**	**0.78**

The phthalocyanine dyes with different metals are ideal for potential Marcus model electron transfer studies (**Figure 3.1)** due to same or similarity of their chemical structures (and therefore same or similar electron transfer reorganizational energies) but different frontier orbitals (and therefore different driving forces for electron transfers). **Figure 3.3** exhibits delocalized pi-electrons in phthalocyanine dyes. **Figure 3.4** exhibits chemical structure and potential structural derivative positions of the phthalocyanine dyes, and **Figure 3.5** exhibits UV-Vis absorption of the phthalocyanine dyes with different metals of this study. The absorption is moving to longer wavelengths as the amount of delocalization increases. When a metal incur more pi-electron delocalization, the smaller the gap between the highest energy π-bonding orbital and the lowest energy π^*-bonding orbital. The phthalocyanine ligand is similar to benzene, but its delocalized electron cloud is much larger due to molecular size. The large central ring is aromatic with 16 π electrons, but the entire macrocycle is also aromatic with 42 π electrons. All of the π electrons are located in delocalized bonding orbitals that cover both sides of the macrocycle plane instead of forming localized double bonds, making the macrocycle very strong.

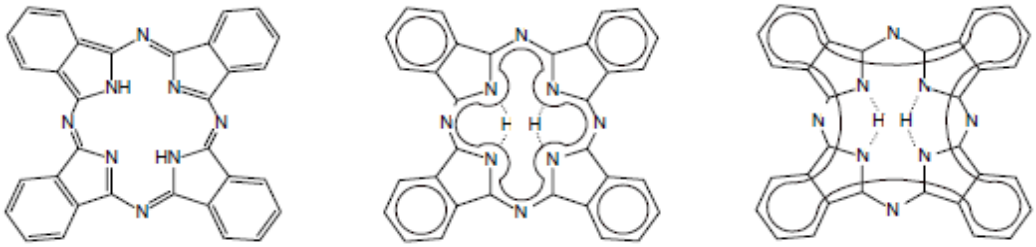

Figure 3.3 Delocalized electrons in a phthalocyanine complex.

Metal Octabutoxy-Phthalocyanines are usually between green and blue in color. The green color of phthalocyanine solutions is a result of multiple different absorption bands in the visible light region, letting only blue, green, and yellow light pass through the solution. The typical absorption bands of metal phthalocyanine complexes of the N absorption band at 250-300 nm ultra-violet range is associated to charge transfer between the phthalocyanine ligand and the metal atom. The B band around violet wavelengths at 300-400 nm (also called Soret absorption) is caused by intramolecular electron π-π* transitions of the macrocycle. The charge transfer band (T band) at the blue wavelengths of 400-450 nm is caused by the charge transfer between the metal atom and an axial ligand. The Q band around red wavelengths at 500-790 nm also arises from an electron π-π* transition in the macrocycle structure. The split Q-band is indicative of a decrease in phthalocyanine symmetry by having two hydrogens at the core. Having a metal in the core affect the symmetry of the phthalocyanine [31].

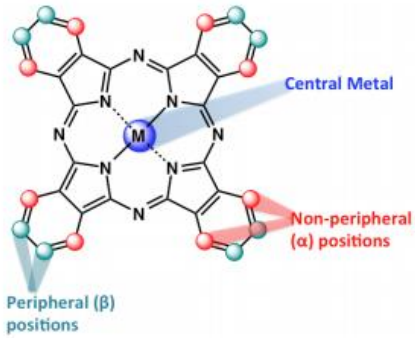

Figure 3.4 Addition of a central metal ion into a phthalocyanine complex.

For some Metal Octabutoxy-Phthalocyanines, less intensive signals are seen in the Q-band due to the formation of dispersed aggregates of the phthalocyanine complex and/or by deformation in the macrocycle structure due to strain caused by the radial substituents of the phthalocyanine macrocycle. Metal Octabutoxy-Phthalocyanine complexes can form bonds with various nitrogen containing functional groups, including amines. The binding occurs between the axial vacancy of the metal center and the lone pair of the nitrogen atom of primary amines and cyclic amines. Several amines are known to bond this way, for example butylamine, propylamine, and pyridine. Secondary aliphatic amines do not bind, due to steric hindrance caused by the wide angle between the substituents. The solvent

DMF, widely used in the synthesis of multiple metal complexes, is a highly polar organic solvent which is capable of coordinating with the axial sites of the active complex. DMF has the ability to limit the aggregation and formation of the active complexes. These metal complexes have eight electro-donating radial butoxy groups that increase the electron density of the macrocycle. The increased electron density does not prevent coordination of amines to the axial vacancies of the complexes.

Figure 3.6 and **Table 3.2** exhibits the frontier HOMO/LUMO orbital levels of the metal Octabutoxy-Phthalocyanines. These frontier orbital values were from measurements of both UV-Vis (where the energy gap were determined) and cyclic voltammetry (CV, where either HOMO or LUMO were determined). Based on frontier orbital profiles, photo induced electron transfer should be from the metal Octabutoxy-Phthalocyanines to P3HT as the LUMOs of the metal Octabutoxy-Phthalocyanines are higher than the LUMO of P3HT, *i.e.*, P3HT is acting as photo doing acceptor. The electron transfer rates can be estimated by the photoluminecense (PL) quenching of the P3HT/dye pair studies in dilute solutions.

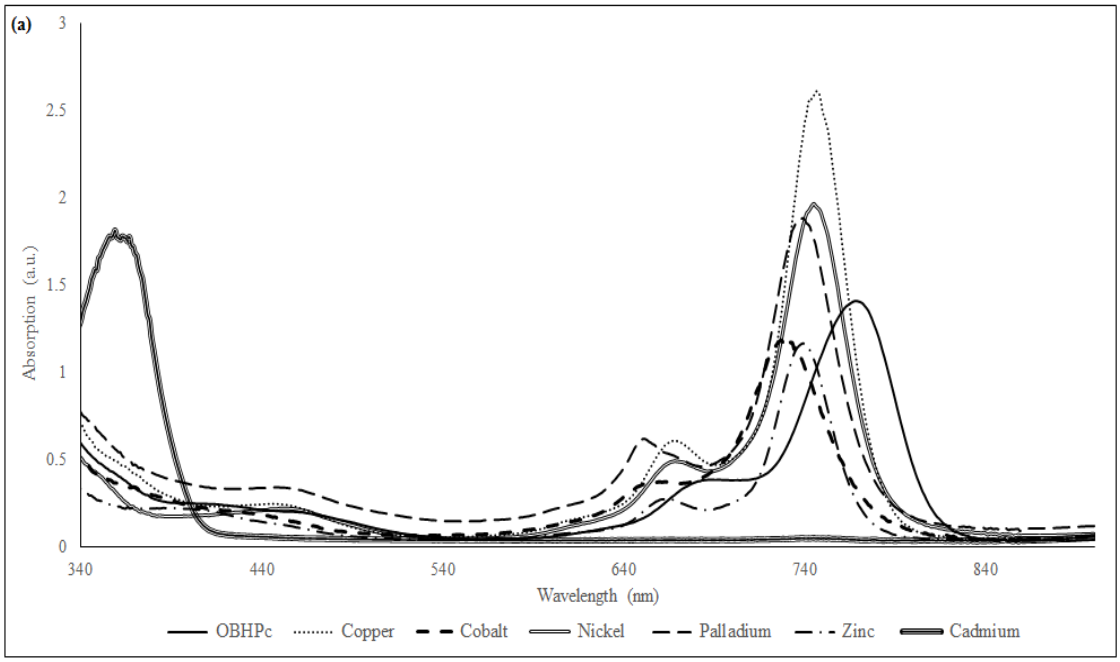

Figure 3.5 (a) UV-Visible absorption spectra of Non-Metalized, Copper, Cobalt, Nickel, Palladium, Zinc, and Cadmium-Substituted Octabutoxy-Phthalocyanines in DMF and (b) UV-Visible absorption spectra of Manganese Octabutoxy-Phthalocyanine in DMF.

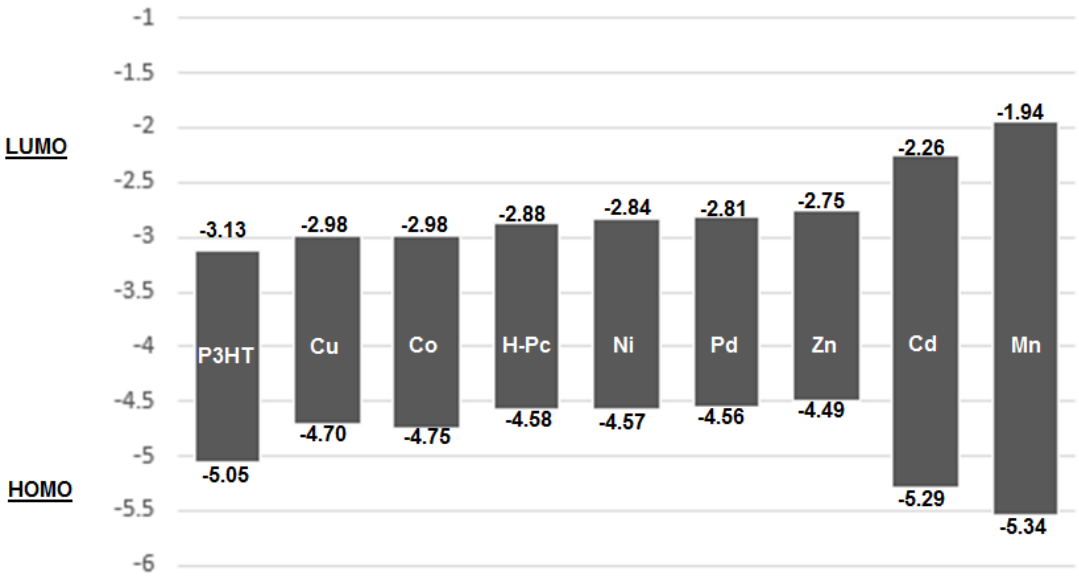

Figure 3.6 Frontier orbital levels of P3HT and eight Metal Octabutoxy-Phthalocyanine dyes.

Table 3.2 Frontier orbital levels and energy gaps of P3HT and eight Metal Octabutoxy-Phthalocyanine dyes, ΔLUMO of each Metal Octabutoxy-Phthalocyanine and P3HT.

	P3HT	Cu	Co	H-OBPc	Ni	Pd	Zn	Cd	Mn
HOMO, eV	-5.05	-4.70	-2.98	-2.88	-4.57	-4.56	-4.49	-5.29	-5.34
LUMO, eV	-3.13	-2.98	-4.75	-4.58	-2.84	-2.81	-2.75	-2.26	-1.94
E_g, eV	1.92	1.72	1.77	1.70	1.73	1.75	1.74	3.03	3.40
ΔLUMO	0	0.146	0.150	0.250	0.289	0.323	0.382	0.872	1.189

The detection of photo-induced PL quenching upon mixing of donor and acceptor provides preliminary evidence that photo-induced charge separation exist and that the two materials might be a suitable donor-acceptor pair for photovoltaic applications. P3HT and the dye complexes both have trend of aggregation with increasing concentration, which affects the emission results significantly. Based on previous studies in our group [32], the aggregation effect was eliminated by a dilute solution and by taking a pure P3HT emission measurement. It was discovered that PL peaks of P3HT non-linearly increased dramatically over the concentration 1×10^{-6} M and reached the point at the concentration of $1\times^{-4}$ M. It was considered via the prior study that polymer P3HT molecules were in unperturbed dimensions status without aggregation. PL quenching peaks presented a line increasing in very dilute concentration under 5×10^{-5} M and non-linear increasing in a high concentration. Therefore, the magnitude of donor and acceptor should be similar. Like the prior publication, to study purely the PL quenching of P3HT by dye without other effect factors,

2.5% w/v P3HT solution and dilute dye solutions (1.2×10^{-4} M, 2.6×10^{-4} M, 4.2×10^{-4} M, and 5.2×10^{-4} M) were used.

Photoluminescent quenching of the P3HT/dye complex pairs in low concentration excited at 450nm was measured. The Stern-Volmer PL quenching coefficients of k_{sv} values of Copper, Cobalt, Non-Metal, Nickel, Palladium, Zinc, Cadmium, and Manganese Octabutoxy-Phthalocyanine were 8.06×10^{3} M^{-1}, 8.07×10^{3} M^{-1}, 8.33×10^{3} M^{-1}, 8.33×10^{3} M^{-1}, 8.33×10^{3} M^{-1}, 1.16×10^{4} M^{-1}, 6.08×10^{4} M^{-1}, and 8.32×10^{3} M^{-1} respectively, and their correlation with LUMO offsets (related to electron transfer driving forces) are exhibited in **Figure 3.7** [34]. The data appears following Marcus electron transfer model, i.e., the normal region is before Cadmium and the 'inverted region' is after the Cadmium.

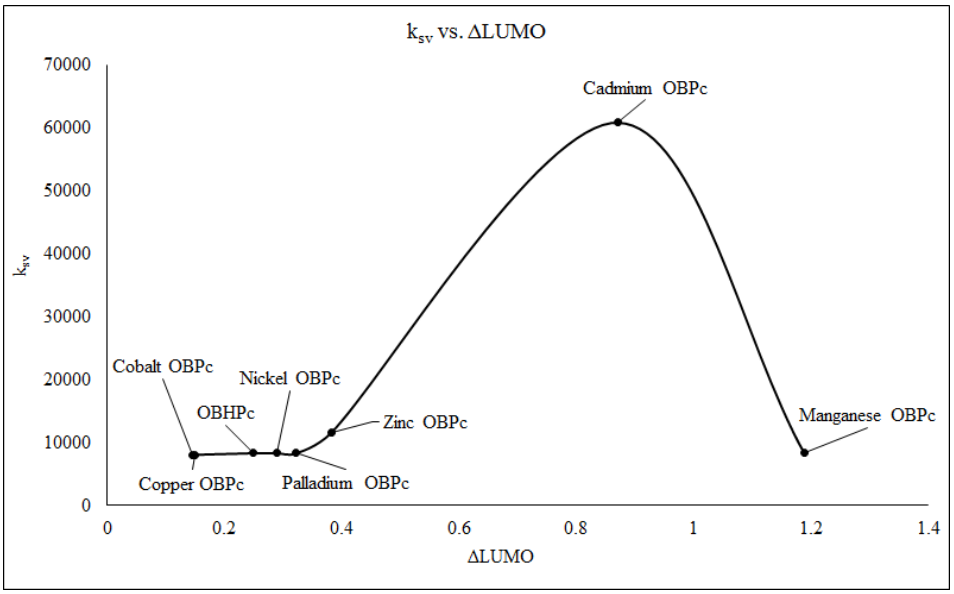

Figure 3.7 The trend of k_{sv} (PL Quenching) vs. ΔLUMO of eight dyes paired with P3HT. Slits of Excitation: 5nm; Emission: 2nm. Excitation wavelength: 440nm. P3HT: 2.5% w/v.

3.3 Summaries and Conclusions

A series of soluble OB-MPc molecular dyes containing different metals have been successfully synthesized and characterized (via NMR, MALDI, electrochemistry, optical absorption and emission spectroscopies, *etc*). These OB-MPc molecular dyes have identical or similar chemical structures but different frontier orbital levels due to different metals present in the center of the molecule, *i.e.*, they are ideal candidates for electron transfer studies as the reorganization energies can be assumed to be same or similar, but the electron transfer driving force would be different. Photoluminescence Stern-Volmer studies of these dyes paired with P3HT were carried out to evaluate photo induced charge separations between the dyes and P3HT. Preliminary results reveal some pattern of Marcus electron transfer curve, *i.e.*, an inverted region was indeed observed.

3.4 Next or Future Research

The next or future research efforts shall include actual optoelectronic device fabrications and characterizations for the P3HT/OB-MPc pair to confirm a similar curve, *i.e*., an optimal solar cell may also exist, and then to covalently attach optimal dyes to a conjugated polymer to achieve most efficient inter-molecular photo induced charge separations, and this may result in high efficient molecular light energy harvesting and conversion systems that are more efficient than natural photo systems.

4. References

[1] Z. Zhuo, F. Zhang, J. Wang, X. Xu, Z. Xu, "Efficiency improvement of polymer solar cells by iodine doping". *Solid State Electron*, 63:83–8 (2011).

[2] P. Tian, L. Tang, J. Xiang, Z. Sun, R. Ji, S. K. Lai, S. P. Lau, J. Kong, J. Zhao, C. Yang, and Y. Li, "Solution processable high-performance infrared organic photodetector by iodine doping", *RSC Advances*, vol. 6, no. 51, pp. 45166–45171 (2016).

[3] Z. Chen, G. Han, L. Yang, L. Cheng, and J. Zou, "Nanostructured thermoelectric materials: Current research and future challenge", *Progress in Natural Science: Materials International*, vol. 22, no. 6, pp. 535–549 (2012).

[4] P. S. Mondal, R. Okazaki, H. Taniguchi, and I. Terasaki, "Photo-Seebeck effect in tetragonal PbO single crystals,"*Journal of Applied Physics*, vol. 114, no. 17, p. 173710 (2013).

[5] Y. Shiraishi, R. Okazaki, H. Taniguchi, and I. Terasaki, "Photo-Seebeck effect in ZnS", *Japanese Journal of Applied Physics*, vol. 54, no. 3, p. 031203 (2015).

[6] Y. Lv, J. Chen, R.-K. Zheng, J. Song, T. Zhang, X. Li, X. Shi, and L. Chen, "Photo-induced enhancement of the power factor of Cu2S thermoelectric films," *Scientific Reports*, vol. 5, no. 1 (2015).

[7] I. Terasaki, R. Okazaki, P. S. Mondal, and Y.-C. Hsieh, "Trials for oxide photo-thermoelectrics," *Materials for Renewable and Sustainable Energy*, vol. 3, no. 3 (2014).

[8] D. Hu, Q. Liu, J. Tisdale, H. Nam, S. Park, H. Wang, A. Urbas, and B. Hu, "Optically tunable Seebeck effect from intramolecular proton-transfer materials in organic vertical thin-film thermoelectric device", *Organic Electronics*, vol. 26, pp. 117–120 (2015).

[9] S. Sun, Chapter 3: Basic Electronic Structures and Charge Carrier Generation in Organic Optoelectronic Materials, in *Introduction to Organic Electronic and Optoelectronic Materials and Devices*, Second Edition, edited by Sun, S. and Dalton, L., CRC Press/Taylor & Francis: Boca Raton, Florida, USA, pp 47-99 (2017).

[10] H. Lee and S. Sun, "Properties and Mechanisms of Iodine Doped P3HT and P3HT/PCBM composites", *Materials Science, 5 (3)*, 479-493 (2018).

[11] E. Lim, K. A. Peterson, G. M. Su, and M. L. Chabinyc, "Thermoelectric Properties of Poly(3-hexylthiophene) (P3HT) Doped with 2,3,5,6-Tetrafluoro-7,7,8,8-tetracyanoquinodimethane (F4TCNQ) by Vapor-Phase Infiltration," *Chemistry of Materials*, vol. 30, no. 3, pp. 998–1010 (2018).

[12] B. Lüssem, M. Riede, and K. Leo, "Doping of Organic Semiconductors,"*Physics of Organic Semiconductors"*, pp. 425–496 (2013).

[13] G. Li, Polymer Self-Organization Enhances Photovoltaic Efficiency. *SPIE Newsroom*: 3–5 (2006).

[14] K. Lim, A. Peterson, G. M. Su, and M. L. Chabinyc, "Thermoelectric Properties of Poly(3-hexylthiophene) (P3HT) Doped with 2,3,5,6-Tetrafluoro-

7,7,8,8-tetracyanoquinodimethane (F4TCNQ) by Vapor-Phase Infiltration," *Chemistry of Materials*, vol. 30, no. 3, pp. 998–1010 (2018).

[15] H.-C. Liao, C.-P. Hsu, M.-C. Wu, C.-F. Lu, and W.-F. Su, "Conjugated Polymer/Nanoparticles Nanocomposites for High Efficient and Real-Time Volatile Organic Compounds Sensors," *Analytical Chemistry*, vol. 85, no. 19, pp. 9305–9311 (2013).

[16] M. Baghgar and M. D. Barnes, "Work Function Modification in P3HT H/J Aggregate Nanostructures Revealed by Kelvin Probe Force Microscopy and Photoluminescence Imaging," *ACS Nano*, vol. 9, no. 7, pp. 7105–7112 (2015).

[17] P. J. Brown, D. S. Thomas, A. Köhler, J. S. Wilson, J.-S. Kim, C. M. Ramsdale, H. Sirringhaus, and R. H. Friend, "Effect of interchain interactions on the absorption and emission of poly(3-hexylthiophene),"*Physical Review B*, vol. 67, no. 6 (2003).

[18] B. Endrődi, J. Mellár, Z. Gingl, C. Visy, and C. Janáky, "Molecular and Supramolecular Parameters Dictating the Thermoelectric Performance of Conducting Polymers: A Case Study Using Poly(3-alkylthiophene)s," *The Journal of Physical Chemistry C*, vol. 119, no. 16, pp. 8472–8479 (2015).

[19] P. Ehrenreich, S. T. Birkhold, E. Zimmermann, H. Hu, K.-D. Kim, J. Weickert, T. Pfadler, and L. Schmidt-Mende, "H-aggregate analysis of P3HT thin films-Capability and limitation of photoluminescence and UV/Vis spectroscopy," *Scientific Reports*, vol. 6, no. 1 (2016).

[20] K. Tashiro, M. Kobayashi, T. Kawai, and K. Yoshino, "Crystal structural change in poly(3-alkyl thiophene)s induced by iodine doping as studied by an organized combination of X-ray diffraction, infrared/Raman spectroscopy and computer simulation techniques," *Polymer*, vol. 38, no. 12, pp. 2867–2879 (1997).

[21] I. Salzmann, G. Heimel, M. Oehzelt, S. Winkler, and N. Koch, "Molecular Electrical Doping of Organic Semiconductors: Fundamental Mechanisms and Emerging Dopant Design Rules,"*Accounts of Chemical Research*, vol. 49, no. 3, pp. 370–378 (2016).

[22] J. Gao, B. W. Stein, A. K. Thomas, J. A. Garcia, J. Yang, M. L. Kirk, and J. K. Grey, "Enhanced Charge Transfer Doping Efficiency in J-Aggregate Poly(3-hexylthiophene) Nanofibers"*The Journal of Physical Chemistry C*, vol. 119, no. 28, pp. 16396–16402 (2015).

[23] M. Glaudell, J. E. Cochran, S. N. Patel, and M. L. Chabinyc, "Impact of the Doping Method on Conductivity and Thermopower in Semiconducting Polythiophenes," *Advanced Energy Materials*, vol. 5, no. 4, p. 1401072 (2014).

[24] J. C. Duda, P. E. Hopkins, Y. Shen, and M. C. Gupta, "Thermal transport in organic semiconducting polymers," *Applied Physics Letters*, vol. 102, no. 25, p. 251912 (2013).

[25] Nguyen, T.; Hasib, M.; Wang, D.; Sun, S, "Design, Synthesis, Characterization, and Optoelectronic Properties of a Novel c-Donor-nc-Bridge-cf-Acceptor Type Block Copolymer", *J. Res. Up. Poly. Sci., 5*, 18-38 (2016) (ISSN: 1929-5995) (DOI:http://dx.doi.org/10.6000/1929-5995.2016.05.01.3).

[26] Hasib, M.; Sun, S, "Effects of Different Bridges of A Series of c-Donor-nc-Bridge-cf- Acceptor Type Block Copolymers for Potential Solar Cell Applications",

J. Res. Up. Poly. Sci., 8, 27-34 (2019) (E-ISSN: 1929-5995/19) (DOI: doi.org/10.6000/1929-5995.2019.08.05).

[27] Sun, S. and Lee, H, "Photoelectric and Thermoelectric Dual Modulation Via a Ternary Composite", *Global Challenge, 3*, 1800077 (2018) (DOI: 10.1002/gch2.201800077)

[28] Lee, H.; Hasib, M.; Sun, S., "Photo-Seebeck Effects in Doped P3HT Composites" *MRS Advance*, Cambridge University Press, *4(8)*, 473-480 (2019) (DOI: https://doi.org/10.1557/adv.2019.94).

[29] Norman, J.; Lee, H.; Sun, S., *"*Polymer Composites for Potential Thermo-Electro Dual Sensors", SPIE Proc. #11096/1109608 (2019), *Organic and Hybrid Sensors and Bioelectronics XII* **(**DOI:10.1117/12.2528941).

[30] Sun, S.; Hasib, M.; Gavrilenko, A.; Devan, J.; Gavrilenko, V., "Bridge Effects on Light Harvesting of a DBfA Type Polymer System", Organic Photovoltaics XVII, Vol. 99421E-1 (2016) (DOI: http://dx.doi.org/10.1117/12.2239027).

[31] Myller, A.T. *The Effect of a Coupling Agent on the Formation of Area-Selective Monolayers of Iron α-Octabutoxy Phthalocyanine on a Nano-Patterned Titanium Dioxide Carrier* (Doctoral Dissertation). University of Eastern Finland. (2016).

[32] Wang, D.; Sun, S., "Optoelectronic Properties of a Series of P3HT/Dye Pairs", *Poly. Sci., 4(2)15,* 1-7 (2018) (DOI: 10.4172/2471-9935.100042)**.**

[33] Lee, H., "Investigation of a Series Doped P3HT Composites for Thermoelectric and Photoelectric Conversions", PhD Dissertation, **2018**, Norfolk State University.

[34] Brookins, S., "Synthesis and Properties of a Series of Metalized Octabutoxy-Phthalocyanine Dyes for Optoelectronic Applications", MS Thesis, **2019**, Norfolk State University.

5. Project Goals and Objectives (From the Proposal)

The short term objectives of this proposed project is to investigate and develop certain molecular, organic, polymeric, or hybrid composite systems (via molecular structure, frontier orbital, and solid state morphology investigation and systematic optimization approaches) for high efficiency photoelectric, thermoelectric, or photo-/thermo-electric multi-functional conversions. The long-term objectives of the project include investigation and elucidation of the fundamental mechanisms of photo- and thermo- induced electron transfer processes in molecular, organic, polymeric, or hybrid materials systems, for instance, the correlations between the molecular structures, frontier orbitals, solid state morphologies, to electron transfers and material bulk photo- and thermo- electric conversions. Another key long term objective is the education and training of future generation scientists on the subject matter.

6. Accomplishment Summaries Under Goals/Objectives

1) Progresses on Investigations of Thermoelectric (TE)/Photoelectric (PE) and Thermoelectric (TE)/Electroelectric (EE) Multi-Functional Materials

The PE/TE and TE/EE dual conversion and dual modulation materials and devices have been preliminary and successfully demonstrated. For example, in one PE/TE dual conversion polymer thin film sample, temperature can effectively modulate the photo detector while simultaneously light can effectively modulate the thermoelectric Seebeck coefficients of the same sample. The correlations of the frontier orbital levels and offsets versus electrical and thermoelectric properties of a series of PCBM:P3HT:dopant ternary composites were also evaluated. It was observed that strong electron accepting strength of the dopant can result in P3HT main chain aggregations even in solution. In the solid-state thin films, it was found that the presence of acceptors increases surface roughness and disrupt the crystallinity of P3HT or P3HT:PCBM thin films. As the orbital offsets (or energy barriers) between HOMO of P3HT and LUMO of dopants increases from F4-TCNQ to iodine to DDQ and finally to TCNQ, the electrical conductivity decreases (possibly due to energy barrier increases), the Seebeck coefficients increases (due to charge carrier density decreases), while the thermoelectric power factor and the thermoelectric figure of merit ZT initially decreases from F4-TCNQ to DDQ (possibly due to dominant electrical conductivity contribution decrease) and then increases slightly to TCNQ (possibly due to dominant Seebeck contribution increase). This work could be helpful to understand the mechanisms of chemical doping of conjugated polymers at the molecular level and their correlations to bulk thermoelectric properties for a variety potential applications.

2) Progresses on Development of a Novel DB-ffA Block Copolymer and Structure/Morphology/Property Correlation Studies of the DBfA Type Block Copolymers

A new benzene disulfide and di-fluorinated monomer **7b** and new disulfide and di-fluorinated functionalized conjugated polymer block **ffA-b** were successfully synthesized and characterized, but once the sulfides were oxidized into the desired sulfone acceptor form, the **ffA-b** become insoluble. Soluble analogues may be developed but that would involve synthetic adjustments from first synthetic step. The correlation studies between chemical structures, morphology, and electronic/optoelectronic properties of the **DBfA** systems that were developed earlier is being evaluated systematically. Important observations/conclusions include that 1) that **DB_1fA** block copolymer containing one methylene unit exhibited the strongest PL quenching and the best optoelectronic property (The PL quenching of no-bridge **DfA** or **DB_2fA** were much less); and 2) an intermediate thin film gran size appear to exhibit best optoelectronic performance in a **DB_1fA** block copolymer.

3) Progresses on Investigations of a Series New Octabutoxy-Metal-Pthalocyannine Complexes (OB-MPc) for Optoelectronics.

A series of soluble OB-MPc molecular dyes containing different metals have been successfully synthesized and characterized (via NMR, MALDI, electrochemistry, optical absorption and emission spectroscopies, *etc*). These OB-MPc molecular dyes have identical or similar chemical structures but different frontier orbital levels due to different metals present in the center of the molecule, *i.e.*, they are ideal candidates for electron transfer studies as the reorganization energies can be assumed to be same or similar, but the electron transfer driving force would be different. Photoluminescence Stern-Volmer studies of these dyes paired with P3HT were carried out to evaluate photo induced charge separations between the dyes and P3HT. Preliminary results confirmed some key features of Marcus electron transfer curve, *i.e.*, an inverted region was indeed observed.

7. Student Training/Education

Though only two graduate and two undergraduate student supports were originally budgeted and allocated in the project, during the entire project period, at least four PhD students, one master student, and over twenty (20) undergraduate students participated and were educated/trained in the awarded project. All participating students are majored in key STEM areas including materials science, chemistry, engineering, *etc*. One PhD degree dissertation (on research thrust 1) and one Master degree thesis (on research thrust 3) have already been completed/defended during the project period. Another PhD dissertation (on research thrust 2) is currently in final stage, and two additional PhD dissertations (on research thrust 1 related subjects) are on the pipeline. Most of the over twenty undergraduate student participants have already graduated with BS degrees in key STEM areas. Majority of the participating students are under-represented minority and/or female students. The first supported PhD graduate student who defended his PhD dissertation in summer 2018 was voted as our materials science PhD program's outstanding PhD student awardee. This PhD graduate has been offered several job offers from major high tech corporations/national labs since his graduation, and most importantly he also successfully won a prestigious NSF postdoctoral research fellow (PRF) grant award (about $100k per year for two years). Recently this PhD graduate accepted a full time position at Sandia National Lab. The one master degree graduate had already been employed by a materials related high tech company before her MS thesis defense in summer 2019. The project supported second PhD student (who is currently preparing his final PhD dissertation defense) has already been offered a full time job at a major high tech company while preparing his final PhD dissertation.

8. Results Dissemination

1) Selected Publications:

[1] Hasib, M.; Sun, S, "Effects of Different Bridges of A Series of c-Donor-nc-Bridge-cf- Acceptor Type Block Copolymers for Potential Solar Cell Applications", *J. Res. Up. Poly. Sci.,* **2019**, *8*, 27-34 (E-ISSN: 1929-5995/19) (DOI: doi.org/10.6000/1929-5995.2019.08.05).

[2] Norman, J.; Lee, H.; Sun, S., *"*Polymer Composites for Potential Thermo-Electro Dual Sensors", SPIE Proc. #11096/1109608, *Organic and Hybrid Sensors and Bioelectronics XII*, **2019 (**DOI:10.1117/12.2528941).

[3] Sun, S. and Hasib, M., *"*Block Copolymer Optoelectronic Property Versus Bridge and Morphology", SPIE Proc. #11074/1109427, *Organic, Hybrid, and Perovskite Photovoltaics XX*, **2019 (**DOI:10.1117/12.2530707).

[4] Montes, J.; Lee, H., Doswell, F.; Sun, S., "Relationship Between Thermoelectric Properties and Morphology of Doped P3HT Thin Films for Potential Thermoelectric Applications", *MRS Advance,* Cambridge University Press, **2019,** *4(30),* 1727-1732 (DOI: https://doi.org/10.1557/adv.2019.324).

[5] Doswell, F.; Lee, H., Montes, J.; Sun, S., "The Effects of Annealing on Doped P3HT Thin Films for Potential Electronic Applications", *MRS Advance,* Cambridge University Press, **2019,** *4(31-32),* 1787-1792 (DOI: https://doi.org/10.1557/adv.2019.281).

[6] Lee, H.; Sun, S., "Photo-Seebeck Effects in Doped P3HT Composites" *MRS Advance*, Cambridge University Press, **2019,** *4(8),* 473-480 (DOI: https://doi.org/10.1557/adv.2019.94).

[7] Sun, S. and Lee, H, "Photoelectric and Thermoelectric Dual Modulation Via a Ternary Composite", *Global Challenge*, **2018,** *3*, 1800077 (DOI: 10.1002/gch2.201800077)

[8] Sun, S. and Lee, H., *"*Polymer Composites for Potential Multi-Function Devices", SPIE Proc. #10738, *Organic and Hybrid Sensors and Bioelectronics XI*, 107381H (1-9), **2018 (**DOI:10.1117/12.2320403).

[9] Wang, D.; Sun, S., "Optoelectronic Properties of a Series of P3HT/Dye Pairs", *Poly. Sci.*, **2018,** *4(2)15*, 1-7 (DOI: 10.4172/2471-9935.100042)**.**

[10] Lee, H.; Sun, S., "Properties and Mechanisms of Iodine Doped P3HT and P3HT/PCBM composites" *Materials Science* (ISSN 2372-0484), American Institute of Mathematical Science (AIMS), **2018**, *5 (3)*, 479-493 (DOI: 10.3934/matersci.2018.3.479)

[11] Lee, H.; Hasib, M.; Sun, S., "Proton radiation studies of conjugated polymer thin films" *MRS Advance,* **2017,** Cambridge University Press (DOI: http://dx.doi.org/10.1557/adv.2017.389).

[12] David, T.; Arasho, W.; Hong, K.; Marder, S.; Smith, O.; Bonner, C.; Sun, S., "Self-Assembly and Charge Transport of a Conjugated Polymer on ITO Substrates", *Poly. Sci.,* **2017**, *vol. 3 (1:1),* 1-8 (DOI: 10.4172/2471-9935.100016).

[13] Lee, H.; Hasib, M.; Sun, S., "Proton radiation effects of conjugated polymer thin films" *Radiation Effects and Defects in Solids,* **2017,** *172:5-6,* 355-363, (DOI: 10.1080/10420150.2017.1336764).

[14] Zhang, C.; Sun, J.; Sun, S, "Synthesis and characterization of poly(3,5-didodecyl-cyclopenta[2,1-b;3,4-b']dithiophen-4-one)", *Synthetic Metals,* **2016**, 221, 275–283 (DOI:10.1016/j.synthmet.2016.09.012)

[15] Sun, S.; Hasib, M.; Gavrilenko, A.; Devan, J.; Gavrilenko, V., "Bridge Effects on Light Harvesting of a DBfA Type Polymer System", Organic Photovoltaics XVII, **2016**, Vol. 99421E-1 (DOI: http://dx.doi.org/10.1117/12.2239027).

[16] Wang, D.; Sun, S., "Synthesis, Characterizations, and Properties of a P3HT-Hemin Covalent System for Solar Energy Conversions", *Poly. Sci,* **2016**, *2(1:9),* 1-8 (DOI: 10.4172/2471-9935.100009).

[17] Nguyen, T.; Hasib, M.; Wang, D.; Sun, S, "Design, Synthesis, Characterization, and Optoelectronic Properties of a Novel c-Donor-nc-Bridge-cf-Acceptor Type Block Copolymer", *J. Res. Up. Poly. Sci.,* **2016**, *5*, 18-38 (ISSN: 1929-5995) (DOI:http://dx.doi.org/10.6000/1929-5995.2016.05.01.3).

[18] Qu, L.; Dai, L.; Sun, S., "Chapter 8: Conjugated Polymers, Fullerene C60, and Carbon Nanotubes for Optoelectronic Devices", in *Introduction to Organic Electronic and Optoelectronic Materials and Devices,* 2nd edition, CRC Press/Taylor & Francis: Boca Raton, Florida, USA, (ISBN# 978-1-4665-8510-2), **2016**.

[19] Sun, S. and Zhang, C., "Chapter 14: Organic and Polymeric Photovoltaic Materials and Devices", in *Introduction to Organic Electronic and Optoelectronic Materials and Devices*, 2nd edition, CRC Press/Taylor & Francis: Boca Raton, Florida, USA, (ISBN# 978-1-4665-8510-2), **2016**.

[20] Sun, S., "Chapter 3: Basic Electronic Structures and Charge Carrier Generation in Organic Optoelectronic Materials", in *Introduction to Organic Electronic and Optoelectronic Materials and Devices*, 2nd edition, CRC Press/Taylor & Francis: Boca Raton, Florida, USA, (ISBN# 978-1-4665-8510-2), **2016**.

[21] Sun, S. and Dalton, L. eds, *Introduction to Organic Electronic and Optoelectronic Materials and Devices*, 2nd Edition, CRC Press/Taylor & Francis: Boca Raton, Florida, USA, **2016**, (CRC book catalog # K19074, ISBN# 978-1-4665-8510-2).

[22] Lee, H., "Investigation of a Series Doped P3HT Composites for Thermoelectric and Photoelectric Conversions", PhD Dissertation, **2018.**

[23] Brookins, S., "Synthesis and Properties of a Series of Metalized Octabutoxy-Phthalocyanine Dyes for Optoelectronic Applications", MS Thesis, **2019.**

2) Selected Presentations/Public Lectures:

1. Sun, S.; Hasib, M., *"*Block Copolymer Optoelectronic Property Versus Bridge and Morphology", paper # 11094-76 in *Organic, Hybrid, and Perovskite Photovoltaics XX* at the International Society for Optical Engineering (SPIE) annual fall convention, San Diego, California, August 11-16, **2019**.
2. Norman, J.; Lee, H.; Sun, S., *"*Polymer Composites for Potential Thermo-Electro Dual Sensors", paper # 11096-08 in *Organic and Hybrid Sensors and Bioelectronics XII*, at the International Society for Optical Engineering (SPIE) annual fall convention, San Diego, California, August 11-16, **2019**.
3. Montes, J.; Lee, H., Doswell, F.; Sun, S., "Relationship Between Thermoelectric Properties and Morphology of Doped P3HT Thin Films for Potential Thermoelectric Applications", presentation of paper # EP13.08, MRS Spring Meeting, April 22-26, **2019**, Phoenix, AZ.
4. Doswell, F.; Lee, H., Montes, J.; Sun, S., "The Effects of Annealing on Doped P3HT Thin Films for Potential Electronic Applications", presentation of paper # EP06.03, MRS Spring Meeting, April 22-26, **2019**, Phoenix, AZ.
5. Hasib, M.; Sun, S., "Optoelectronic properties versus bridge interfaces of a series DBpfA type block copolymers", an oral presentation paper # PMSE-156 (ID: 3108475), ACS Spring National Convention, Orlando, FL, March 31-April 4, **2019**.
6. Sun, S. and Lee, H., "Photo-Seebeck Effects in Doped P3HT Composite", presentation of paper # 3038277, 2018 MRS Fall Meeting, November 23-27, **2018** in Boston, MA.
7. Sun, S. and Lee, H., *"*Polymer Composites for Potential Multi-Function Devices", paper # 10738-54 in *Organic and Hybrid Sensors and Bioelectronics XI*, at the International Society for Optical Engineering (SPIE) annual fall convention, San Diego, California, August 19-24, **2018**.
8. Sun, S. "The Sun and the Energy", an invited guest speaker at the 2018 career day, April 18, **2018**, Hardy Elementary School, Smithfield, Virginia, USA.
9. Lee, H. O. & Sun, S.-S. *"Doping Studies of P3HT:PCBM with Iodine"* AAAS Emerging Researchers National (ERN) Conference in STEM, February 22-24, **2018**, Washington D.C.
10. Lee, H.; Sun, S., "Iodine Doping Studies of P3HT/PCBM", presentation of paper # 2802451, 2017 MRS Fall Meeting, November 30, **2017** in Boston, MA.
11. Sun, S.; Wang, D., "Conjugated polymer-dye weakly coupled covalent assembly for optoelectronics", an oral presentation paper # POLY-733, ACS Fall National Convention Meeting 254, Washington DC, August 20-24, **2017**.
12. David, T.; Arasho, W.; Smith, O.; Hong, K.; Bonner, C.; Sun, S. "Chemical and Charge Transfer Studies on Interfaces of a Conjugated polymer and ITO", paper # 10348-53 in *Physical Chemistry of Semiconductor Materials and Interfaces XVI*, at the International Society for Optical Engineering (SPIE) annual fall convention, San Diego, California, August 6-10, **2017**.
13. Sun, S. and Lee, H., *"*Proton radiation effects of conjugated polymer composite thin films", paper # 10363-75 in *Organic, Hybrid, and Perovskite Photovoltaics XVIII*, at the International Society for Optical Engineering (SPIE) annual fall convention, San Diego, California, August 6-10, **2017**.

14. Lee, H.; Hasib, M.; Sun, S., "Proton Radiation Studies on Conjugated Polymer Thin Films", presentation of paper # ED8-2632698, 2017 MRS Spring Meeting, April 17-21, **2017** in Phoenix, Arizona.
15. Sun, S.; Hasib, M.; and Nguyen, T., "Development and studies of DBfA/DfA block copolymers for optoelectronics", an oral presentation paper # PMSE-90, ACS Spring National Convention Meeting 253, San Francisco, CA, April 2-6, **2017**.
16. Sun, S.; Hasib, M., "Light Harvesting via a DBA Type Polymer System", presentation at the 2016 Solar Energy Research Center (SERC) annual conference at University of North Carolina (UNC), Chapel Hill, NC, October 20-21, **2016**.
17. Sun, S.; Hasib, M.; Gavrilenko, A.; Devan, J.; Gavrilenko, V., "Bridge Effects on Light Harvesting of Donor-Bridge-Acceptor Type Polymer Systems", *Organic Photovoltaics XVII*, paper # 9942-53 at the International Society for Optical Engineering (SPIE) annual fall convention, San Diego, California, August 28-31, **2016**.
18. Hasib, M. and Sun, S., "Optoelectronic Properties of a DBfA Type Block Copolymer", an oral presentation with paper # 2402878, ACS spring national convention, Meeting 251, San Diego, CA, March 13-17, **2016**.

9. Honors and Awards

During the project period, the project PI typically was awarded 1-2 faculty related honors/awards/certificates from the awardee organizational units every year, examples of the honors/awards/certificates include "Outstanding Researcher of the Year", "Outstanding Student Research Mentor of the Year", or "Outstanding Faculty Scholarship of the Year", *etc*. PI also won a research instrumentation award titled "Infrastructure Enhancement of Soft Materials Research/Education at NSU" (DOD Award # W911-NF-17-1-0450), and as a co-PI jointly won an NSF-CREST center grant award titled "CREST Center for Renewable Energy and Advanced Materials (CREAM)" (NSF Award # HRD-1547771). Most importantly, one of PI's PhD student mentees was voted as the outstanding PhD student awardee in 2018 at the awardee organization, and that same PhD graduate also successfully won a prestigious NSF postdoctoral research fellow (PRF) grant award (about $100k per year for two years).